 https://doi.org/10.3311/PPci.23600

Periodica Polytechnica Civil Engineering, 68(4), pp. 1328–1349, 2024

The Effect of Nonlinear Sloshing Response of Water on Seismic Behavior of Reinforced Concrete Elevated Water Tanks

Olgun Köksal[1], Zeki Karaca[2], Erdem Türkeli[3*]

[1] Construction Department, Vocational School, Samsun University, Mehtmetpaşa District, 16. Street 10, 55850 Kavak, Samsun, Türkiye
[2] Department of Civil Engineering, Faculty of Engineering, Ondokuz Mayis University, Körfez District 64, 55270 Atakum, Samsun, Türkiye
[3] Construction Department, Vocational School of Technical Sciences, Ordu University, Akyazı District, 15 Temmuz Milli İrade Blv., Çiğdem Street 9, 52200 Altınordu, Ordu, Türkiye
* Corresponding author, e-mail: erdemturkeli@odu.edu.tr

Received: 08 October 2023, Accepted: 12 June 2024, Published online: 15 July 2024

Abstract

In this study, the fluid-structure interactive behavior by using the Westergaard approach and the Smoothed Particle Hydrodynamics (SPH) method of a 1000 m^3 reinforced concrete (RC) elevated water tank under different seismic activities i.e., Kocaeli, Van, Kahramanmaraş and Kobe earthquakes was investigated. In the SPH method, the resulting hydrodynamic pressures were applied to the interior of the wall of the structure as an external force which is made as mass additions to the tank walls in Westergaard approach. With the help of software developed, the load carrying system of the elevated water tank was modeled using the MATLAB Partial Differential Equation Toolbox (PDE) software, based on the finite element method, and its verification was made by comparing with ANSYS software model. Dynamic condensation method was used to perform time history analyses for the cited earthquakes. The time-dependent solutions of partial differential equations are solved with the help of ODE45 functions based on Runge-Kutta method, by arranging the equation of motion in state-space format. The cited tank was analyzed linearly under different seismic activities for empty, half-filled (50%) and full-filled (100%) cases and the obtained results were compared with each other. It has been concluded that considering nonlinear behavior of the fluid during the earthquake with the SPH method provided consistency with the real behavior of RC elevated water tanks and gave more realistic results than the traditional Westergaard approach.

Keywords

nonlinear, sloshing, smoothed particle hydrodynamics, elevated water tank

1 Introduction

With the increase in population in recent years, it is observed that consumption habits have changed rapidly. Water, which is used as a basic food item, is also used in agriculture, livestock, industry, forestry, clothing, etc. It is frequently consumed in the production of new products in many areas. The structures used to obtain and store clean water have been continuously developed throughout human history. For this purpose, many historical structures such as cisterns, fountains, aqueducts, water channels were needed. Today, large volumes of tanks can be built by using materials such as RC, steel, etc. to store water. Recessed tanks are used below the ground level, and above-ground tanks are used just above the ground level. However, in areas where the city main pressure is not sufficient, the use of elevated water tanks becomes a necessity. In addition, the use of water, which is a basic need after natural events such as earthquakes and floods, gains even more importance. For this reason, it is necessary that the elevated water tanks (where water is stored) after the earthquake should not be damaged and the use of these structures should be maintained. However, it was observed that the water tanks were damaged in Chile earthquake in 1960 [1], Izu-Oshima and Miyagi earthquakes in 1978 [2], Whittier earthquake in 1987 [3] and Kahramanmaraş earthquake in 2023 [4] among others. In addition, it is understood that the fluid-structure interaction in the earthquake behavior of elevated water tanks should be handled with more realistic methods. Elevated water tanks consist of columns, beams, truncated cones and cylinders. For this reason, the seismic behavior of these elevated tanks and the seismic behavior

Cite this article as: Köksal, O., Karaca, Z., Türkeli, E. "The Effect of Nonlinear Sloshing Response of Water on Seismic Behavior of Reinforced Concrete Elevated Water Tanks", Periodica Polytechnica Civil Engineering, 68(4), pp. 1328–1349, 2024. https://doi.org/10.3311/PPci.23600

of recessed tanks differ from each other. The convective and impulse behaviors of an elevated water tank containing fluid are also different from other tanks under the influence of earthquakes. For this reason, many researchers have studies on the fluid-structure interaction of elevated water tanks. Researches on liquid tanks, began at the end of the 19th century, still continue in parallel with the development of technology. When the technical literature is examined in details, the studies on elevated water tanks are as follows.

There are studies in which the convection of water in the tank is not considered and the water mass is accepted as a single mass [5], studies utilizing multi-mass system approach [6, 7], studies taking into account the added mass approach [8]. In these cited studies, pressures acting on the wall of the tank occurred in a static state which is defined as hydrostatic. However, seismic activities occurred on the ground caused the water in tank oscillate and agitate. In this situation, the pressure of the water exerted on the wall of water tank becomes hydrodynamic. Also, the water in the tank oscillates and agitates that the water displays more different behavior compared with the main load carrying system of the elevated water tank. In order to perform dynamic seismic calculations of elevated water tanks, the convection of the stored water and the convective resulted hydrodynamic pressures as close to real situation as possible should be taken into account. For this, there are many methods such as Westergaard method [9], Hoskins and Jacobsen method [10], Werner-Sundguist method [11], Housner method [6] and Haroun method [5]. There are also mesh dependent (Finite Element Method, Finite Volume Method) or mesh independent methods. In these studies, a mesh is formed by accepting liquid a finite element and the dynamic behavior is modeled in this way. However, there are various difficulties when performing time history analyzes in these models. In mesh independent methods, modeling is performed by considering the liquid as a particle. Based on the Lagrangian approach, the nonlinear particle motion of the liquid was investigated using the Smoothed Particle Hydrodynamic (SPH) method [12–14]. There are many studies examining the behavior of tanks under dynamic effects [15-19]. Also, besides the studies given above, Tavakoli and Ahmadi [20] studied about the effect of impact loading (weighing about 100 kg TNT) on three cylindrical concrete water tanks. Tiwari and Hora [21] modelled a RC elevated water tank in ANSYS [22] to evaluate the principal stresses in different parts of the tank by considering soil-structure interaction. Jaiprakash Chitte et al. [23] studied about the seismic response of RC elevated water tanks by considering the effect of the response reduction factor "*R*". Martínez-Martín et al. [24] studied about the seismically optimization and design of RC water storage tanks. Mansour and Nazri [25] considered the effect of fluid-structure interaction of frame-type supporting structures for elevated water tanks on seismic response.

As it can be seen from the detailed technical literature research above, no studies were found in which the modeling of the water in elevated tanks according to the SPH method considering nonlinear sloshing. For this reason, in this study, the behavior of a selected and structurally verified RC elevated water tank under the influence of seismic excitation is investigated based on the Westergaard approach and SPH method (considering the nonlinear sloshing of the water). A software has been developed in MATLAB [26] programming language for situations that prolong the time history analysis, such as changes in hydrodynamic water pressures and excess number of finite elements in each time step. Also, in these situations, the computer's memory is insufficient. By this developed software, even on personal computers, seismic time history analyzes of RC elevated water tanks can be performed taking into account the linear and nonlinear behavior of water.

2 Material and method

2.1 Fluid-structure system modeling

In this study, the two methods presented below are used in the fluid-structure analysis of the cited RC elevated water tank under seismic loads and the results are compared with each other.

2.1.1 Westergaard method

Hydrodynamic pressure distribution can be examined with the Westergaard approach, which is also used in elevated water tanks. The Westergaard approach assumes that the fluid is inviscous and compressible, surface waves are negligible, ground motion is harmonic, and displacements are small. In this approach, a solution is obtained by adding the liquid mass to the tank wall at appropriate heights according to the hydrodynamic pressure distribution [9, 27].

Equation (1) describes the motion of a multi-degree-of-freedom system due to earthquake ground motion:

$$[\boldsymbol{M}]\ddot{u}+[\boldsymbol{C}]\dot{u}+[\boldsymbol{K}]u=-[\boldsymbol{M}]\ddot{u}_g(t). \quad (1)$$

In Eq. (1), [$\boldsymbol{M}$] is the mass matrix, [$\boldsymbol{C}$] is the damping matrix, [$\boldsymbol{K}$] the stiffness matrix, $\ddot{u}$ is the relative acceleration, $\dot{u}$ relative velocity, u relative displacement, $\ddot{u}_g(t)$ is

the ground motion acceleration. In added mass approach, Eq. (1) becomes Eq. (2):

$$[M]\times\ddot{u}+[C]\dot{u}+[K]u=-[M]\times\ddot{u}_g(t). \quad (2)$$

From Eq. (2), it can be deducted that the mass has increased yet the stiffness and damping have not.

In 1931, Westergaard expressed the hydrodynamic pressure distributions on dams. In Fig. 1, the change in hydrodynamic pressure with wall height according to the Westergaard approach is shown [9, 27].

The hydrodynamic pressure according to Westergaard approach can be found with Eq. (3):

$$P_i(z)=\frac{7}{8}\times a_m\times\rho\times\sqrt{h\times z}. \quad (3)$$

In Eq. (3), P_i indicates the hydrodynamic pressures resulting from the impulse effect, ρ represents the unit volume mass of the liquid, and a_m indicates the maximum ground motion acceleration.

2.1.2 Smoothed Particle Hydrodynamics (SPH) method

As cited before, in order to determine hydrodynamic pressures, there are many methods. Among these methods, Smoothed Particle Hydrodynamics (SPH) method is the widely preferred and used [28]. In the area of computational fluid mechanics, in which the flow of fluid particles and the interaction with structures is represented, SPH method can be used effectively. Also, this method depends on the Lagrangian approach in which large deformations are obtained. To solve astrophysics problems, this method is firstly utilized by Monaghan [12] and Lucy [29]. Also, SPH method is utilized by many researchers [12–15, 28–31]. In SPH method, the fluid is accepted as a particle in order to figure out the numerical equations of fluid dynamics. SPH is a preferred method in many areas for the modelling of fluids today since the fluid can be generated in the desired geometry. Various particle clusters are organized by determining an interpolation function (Kernel function) [15, 29] based on the SPH Langrange approach.

In fluid dynamics, by utilizing the Navier-Stokes equations, the integration of each particle in the fluid model can be performed based on the physical properties around the radius *r*. "*h*" is the interpolation length, determines the adjoining array of particles surrounding *r*. At the certain period of each time step, new physical values are determined and transferred to the updated new values (Fig. 2).

In each time step, by utilizing the Kernel function, the Navier-Stokes momentum equations, continuity equation and equation of state are determined depending on the weight of any particle. Because of the reason that the conservation equations of the Kernel function are hoped to come out possible values based on the interpolation function at any point, the cited function is transformed to a differential form in relevance with the particle. By this way, the displacement of the particle in time can be simulated.

In fluid dynamics, partial differential equations can be utilized in case where the flow problem contains nonlinearity. Because of the reason that Lagrangian approximation is based upon SPH method that is not dependent on meshing, the assumption of finite number of particles can be applied to model a certain volume of fluid. In these particles, the own mass and any physical properties can be transferred. The motion of the particle can be calculated by Eq. (4) [11, 12, 15]:

$$F(r)=\int_{\Omega}F(r')W(r-r',h)dr. \quad (4)$$

In Eq. (4), *r*, *r*′, Ω, *W* and *h* are denoting the place where variable F is determined, the location where the variable is known, the area of solution, the weight function and the action distance of the weight function, respectively. Also,

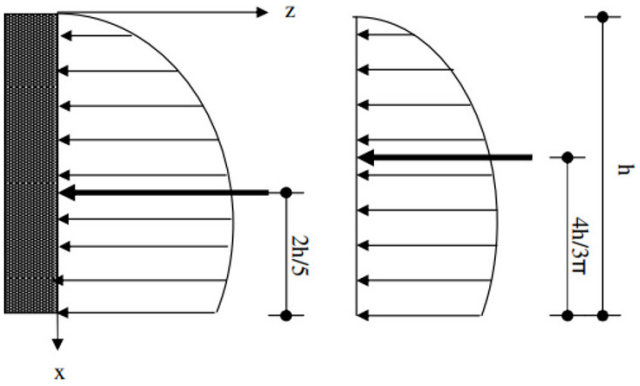

Fig. 1 Hydrodynamic pressure distributions along the wall height according to the Westergaard approach [9, 27]

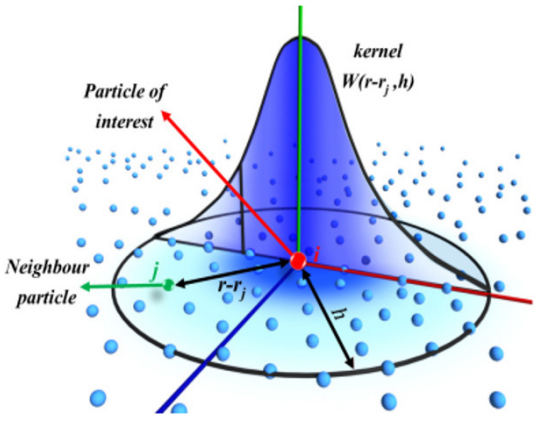

Fig. 2 *W*(*r*) The principle of the SPH kernel function [14]

in Eq. (4), $W(r-r', h)$ is defined as the Kernel function cited above. Depending on the set of particles, the function F can be determined in a discrete manner. In such case, the interpolation of function on a particle takes place and becomes to a sum on all particles along the interpolation length h (Eq. (5)) [11, 12, 15]:

$$F(r_a) \approx \sum_b F(r_b) W(r_a - r_b, h) \Delta v_b, \tag{5}$$

where $v_b = m_b/\rho_b$ is denoting the adjacent particle in which m_b and ρ_b are denoting the mass and the density of the particle. By this way, Eq. (5) turned to:

$$F(r_a) \approx \sum_b F(r_b) \frac{m_b}{\rho_b} W(r_a - r_b, h). \tag{6}$$

The precision of the model produced by using SPH method is dependent on the fine selection of the Kernel function [14]. In this study, Eq. (7) is utilized as the Kernel function:

$$W(q) = \alpha_D \left(1 - \frac{q}{2}\right)^4 (2q+1), \ 0 \le q \le 2, \tag{7}$$

where α_D = $21/164\pi h^3$ in three dimensions. Depending on the provided r/h ratio, q is defined as the dimensionless distance between particles a and b. Equation (8) can be utilized to express the conservation of momentum in a continuous medium [14]:

$$\frac{dv}{dt} = -\frac{1}{\rho} \nabla P + g + \Gamma, \tag{8}$$

in which Γ is expressed as viscous force. Also, g is defining gravitational acceleration. In order to define the acceleration of a particle due to the interaction with an adjoining particle, momentum equation in SPH method given with Eq. (9) is utilized [15]:

$$\frac{dv_a}{dt} = -\sum_b m_b \left(\frac{P_a + P_b}{\rho_a + \rho_b} + \Pi_{ab} \right) \nabla_a W_{ab} + g, \tag{9}$$

in which Π_{ab} (given with Eq. (10)) is expressing the viscous terms between particles a and b:

$$\Pi_{ab} = \begin{cases} \dfrac{-\alpha \overline{c_{ab}} \mu_{ab}}{\overline{\rho_{ab}}} & v_{ab} \times r_{ab} < 0 \\ 0 & v_{ab} \times r_{ab} > 0 \end{cases}, \tag{10}$$

in which $r_{ab} = r_a - r_b$ is expressing the coordinates of particles. Also, $v_{ab} = v_a - v_b$ is denoting the viscosity. $\overline{c_{ab}} = 0.5(c_a - c_b)$ is expressing the particles' average sound velocity. Additionally, $\eta^2 = 0.01\ h^2$ and α are chosen as suitable parameters to provide the propagation ($\alpha = 0.01$). Equation (11) can be utilized to express the continuity equation of a weakly compressible fluid [15]:

$$\frac{d\rho_a}{dt} = \rho_a \sum_b \frac{m_b}{\rho_b} v_{ab} \nabla_a W_{ab}. \tag{11}$$

Because of the reason that the fluid is assumed as weakly compressible in SPH method, Eq. (12) can be used to calculate the pressure value of the fluid [15]:

$$P = b \left[\left(\frac{\rho_a}{\rho_0} \right)^\gamma - 1 \right], \tag{12}$$

$b = c_0^2 \rho_0 / \lambda$ is dependent on the elasticity modulus of the fluid and the value of b is constant. Also, ρ_0 is the specific mass of water whose value is ρ_0 = 1000 kg/m^3. In Eq.(12), γ can be taken between 1 to 7 (γ = 7). Moreover, "−1" in Eq. (12) represents that the pressure on the free surface of the fluid is zero. For wave height:

$$d_{\max} \le 0.2R \text{ and } d_{\max} \le 0.2h, \tag{13}$$

conditions given in Eq. (13) must be met. If these conditions are not met, nonlinear effects should be taken into account [27]. In this study, since these conditions were not met, the nonlinear effect of water was taken into account by using SPH method.

2.2 MATLAB Partial Differential Equation (PDE) Toolbox

The MATLAB Partial Differential Equation (PDE) Toolbox uses functions to solve general PDEs, heat transfer and structural mechanics by using FEM [26].

Features of this toolbox:

- It can be used to calculate deformations and stresses.
- The time-integrating solver provides users to model dynamical and vibrational behavior of the structure.
- In the toolbox, modal analysis can be performed to obtain natural frequencies and mode shapes.
- In the toolbox, heat distributions, heat flow and heat flow rates over surfaces can be calculated by modeling conductive heat transfer problems.
- Diffusion, electrostatics, magnetostatics and special PDEs can be solved.
- Standard Triangle Language (STL) is utilized to import two-dimensional and three-dimensional geometries. Also, by using triangular and tetrahedral elements, meshes can be created.

By using Eqs. (14) to (16), eigenvalue problems can be solved:

$$m\frac{\partial^2 u}{\partial t^2}+d\frac{\partial u}{\partial t}-\nabla\times\left(c\nabla u\right)+au=f, \tag{14}$$

$$\nabla\times\left(c\nabla u\right)+au=\lambda du, \tag{15}$$

$$-\nabla\times\left(c\nabla u\right)+au=\lambda^2 mu. \tag{16}$$

In solving eigenvalue problems, the coefficients m, d, c, a and f is not dependent on the solution u or its gradient. When solving PDEs, there are two boundary choices for each edge or face. Dirichlet boundary conditions realize the solution equation at the edge or surface [26]:

$$hu=r. \tag{17}$$

Here, h and r are three-dimensional (x, y, z) space functions. Generalized Neumann boundary conditions perform the solution equation at the edge or surface:

$$\boldsymbol{n}\times\left(c\nabla u\right)+qu=g, \tag{18}$$

where $\boldsymbol{n}$ is the unit normal vector, q and g are functions defined in $\partial\Omega$ depending on (x, y, z) in three-dimensional space. In linear elasticity, the stiffness matrix of an isotropic material depends on two parameters, E, representing Young's modulus and v, Poisson's ratio. Equilibrium equation in static condition is given as:

$$-\nabla\times\sigma=f. \tag{19}$$

The relationship between linearized small displacements and strains is as follows [26]:

$$\varepsilon=\frac{1}{2}\left(\nabla_u+\nabla_u^T\right). \tag{20}$$

The angular momentum equilibrium shows that the stress is symmetrical:

$$\sigma_{ij}=\sigma_{ji}. \tag{21}$$

The Drucker-Prager criterion [32] is used to create the yield surface or flow function of materials. This criterion is also used to determine the limit of linear and non-linear behavior in structural systems with RC material. The Drucker-Prager yield criterion is expressed by Eq. (22):

$$F\left(\sigma_{ij}\right)=\alpha I_1+\sqrt{J_2}-k. \tag{22}$$

Here, I_1 the hydrostatic component or first invariant of the stress tensor is:

$$I_1=\boldsymbol{\sigma}_{xx}+\boldsymbol{\sigma}_{yy}+\boldsymbol{\sigma}_{zz}. \tag{23}$$

J_2 second invariant of deviatoric stress tensor:

$$J_2=\frac{1}{6}\left[\left(\boldsymbol{\sigma}_{xx}-\boldsymbol{\sigma}_{yy}\right)^2+\left(\boldsymbol{\sigma}_{yy}-\boldsymbol{\sigma}_{zz}\right)^2+\left(\boldsymbol{\sigma}_{zz}-\boldsymbol{\sigma}_{xx}\right)^2\right] +\boldsymbol{\tau}_{xy}^2+\boldsymbol{\tau}_{yz}^2+\boldsymbol{\tau}_{zx}^2. \tag{24}$$

In Eq. (24), $\boldsymbol{\sigma}_{xx}$, $\boldsymbol{\sigma}_{yy}$ and $\boldsymbol{\sigma}_{zz}$ are normal stresses along x, y and z directions, respectively. Also, $\boldsymbol{\tau}_{xy}$, $\boldsymbol{\tau}_{yz}$ and $\boldsymbol{\tau}_{zx}$ are shear stresses on the x-plane in y direction, y-plane in z direction and z-plane in x direction, respectively.

α and k indicate the material constants of the Mohr-Coulumb criterion, which depend on the cohesion angle c and the internal friction angle ϕ.

$$\alpha=\frac{2\sin\phi}{\sqrt{3\left(3-\sin\phi\right)}} \tag{25}$$

$$k=\frac{6c\cos\phi}{\sqrt{3\left(3-\sin\phi\right)}} \tag{26}$$

c and ϕ are expressed below with the axial tensile stress of concrete f_t' and axial compressive stress of concrete f_c' as follows:

$$\sin\phi=\frac{f_c'-f_t'}{f_c'+f_t'}, \tag{27}$$

$$c=\frac{f_c'f_t'}{f_c'-f_t'}\tan\phi. \tag{28}$$

In this study, Mohr-Coulomb material constants c = 3N/mm^2, $\phi = 32^0$ are assumed.

2.3 Dynamic condensation

In this study, due to the size of the matrix (mass and stiffness matrix) and the insufficient capacity of conventional computers, the dynamic condensation method was used while analyzing the elevated water tank in the time history analysis, and the details of the method are given below [33, 34].

In Eq. (29), the joint equation of motion for the damped state of structural systems under ground motion can be written:

$$\left[\boldsymbol{M}\right]\left\{\ddot{U}\right\}+\left[\boldsymbol{C}\right]\left\{\dot{U}\right\}+\left[\boldsymbol{K}\right]\left\{U\right\}=\left\{F\right\}. \tag{29}$$

Here, [M], [C], [K] are denoting mass, damping and stiffness matrices of the system, respectively. Also, $\{\ddot{U}\}$, $\{\dot{U}\}$, $\{U\}$, $\{F\}$ are denoting the total acceleration, velocity, displacement and external load vectors, respectively.

$$[\boldsymbol{M}_r]\{\ddot{u}\}+[\boldsymbol{C}_r]\{\dot{u}\}+[\boldsymbol{K}_r]\{u\}=\{F_r\} \tag{30}$$

The reduced mass, damping, stiffness matrices and external force vector are given in Eqs. (31)–(34), respectively [33, 35, 36]:

$$[\boldsymbol{M}_r]=[T]^T[\boldsymbol{M}]\{T\}, \tag{31}$$

$$[\boldsymbol{C}_r]=[T]^T[\boldsymbol{C}]\{T\}, \tag{32}$$

$$[\boldsymbol{K}_r]=[T]^T[\boldsymbol{K}]\{T\}, \tag{33}$$

$$\{F_r\}=[T]^T\{F\}. \tag{34}$$

Rayleigh damping (Fig. 3) $[\boldsymbol{C}] = \alpha[\boldsymbol{M}] + \beta[\boldsymbol{K}]$ is expressed as follows in Eq. (35):

$$\frac{1}{2}\begin{bmatrix}\frac{1}{\omega_i} & \omega_i\\ \frac{1}{\omega_i} & \omega_j\end{bmatrix}\begin{Bmatrix}\alpha\\ \beta\end{Bmatrix}=\begin{Bmatrix}\xi_i\\ \xi_j\end{Bmatrix}, \tag{35}$$

where ω_i, ω_j, ξ_i, ξ_j are the natural frequencies and damping ratios for the i^{th} and j^{th} modes. The α and β coefficients were calculated by assuming the required damping ratio of 5% for the Rayleigh damping matrix [36, 37]. Also, in this study, the damping ratio of the fluid is considered as 0.5% in the SPH analysis. ODE45 MATLAB tools based on the Runge-Kutta method were used to solve the above equations of motion [26].

3 Application

3.1 Description of the RC elevated water tank

In this study, the behavior of the 1000 m^3 RC elevated water tank (Fig. 4) [38] selected from the technical literature

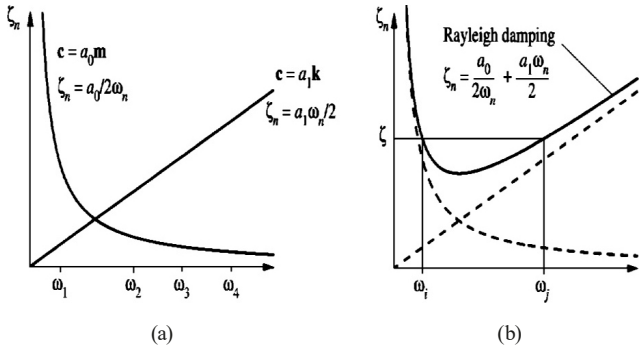

Fig. 3 Variation of modal damping ratios with natural frequency; (a) mass and stiffness proportional damping (b) Rayleigh damping [37]

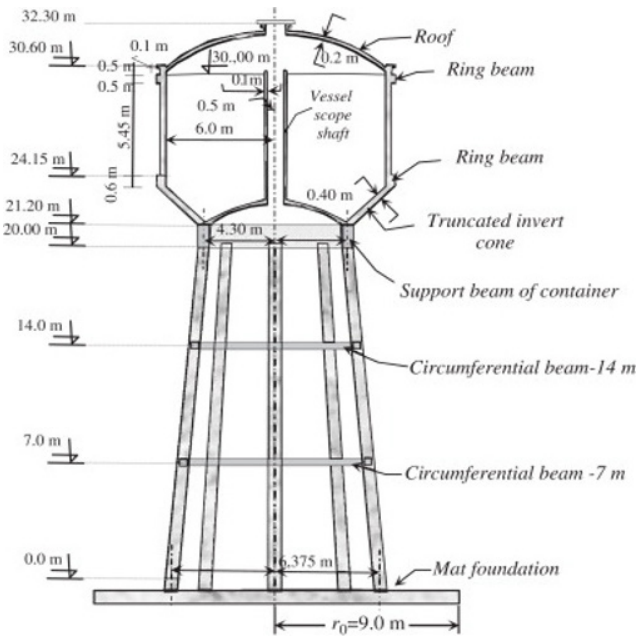

Fig. 4 Vertical section and details of the 1000 m^3 RC elevated water tank [38]

under the effect of earthquake ground motions is examined. The load carrying system of the RC elevated water tank (frame supporting structure) consists of columns, pillow beams, conical part and cylindrical part. Columns are 83.5 cm × 75 cm rectangular section, pillow beams are 35 cm × 35 cm square section, and the reservoir thickness is 40 cm. In the case where water level at the tank is 100% full (30.35 m from the ground), the height of water is 9.25 m. By the same way, in the case where water level at the tank is 50% full (25.73 m from the ground), the height of water is 4.63 m [39].

In Tables 1 and 2 [38, 40], the main geometrical and material properties of the cited water tank is provided, respectively.

3.2 Finite element model of RC elevated water tank

The load carrying system of the RC elevated water tank is modeled on the basis of the finite element method. In the modeling, three-dimensional solid tetrahedral finite element is preferred for both the frame elements (columns, beams) and the surface load carrying elements. Finite element mesh is created using MATLAB PDE toolbox [26]. Based on the finite element method, this toolbox can calculate the stresses and deformations that occur as a result of static and dynamic analysis of the structural system. This toolbox, which performs the structural dynamics calculation model and vibration modeling, has a solver that performs direct time integration. Modal analysis can be performed to obtain natural frequencies and mode shapes.

Table 1 Geometrical properties of cited RC elevated water tank [38]

Water tank vessel properties	
	Dimensions
Vessel volume	1000 m^3
Inner diameter	12 m
Height	10.6 m
Top ring beam	0.6 m × 0.6 m
Bottom ring beam	0.8 m × 0.6 m
Vessel thickness	0.20 m
Bottom slab thickness	0.50 m
Roof thickness	0.20 m
Water tank staging properties	
Column dimensions	0.835 m × 0.75 m
Column height	20 m
Staging inner diameter in the top	8.60
Staging inner diameter in the bottom	12.75
Beams dimensions	0.35 m × 0.35 m

Table 2 Material properties of the cited RC elevated water tank [40]

Material	Class	Modulus of elasticity (GPa)	Poisson ratio	Weight of volume unit (kN/m^3)
Concrete	C25	30	0.18	23
Steel	S420	210	0.30	78.5

There are 11051 finite elements and 3894 nodes in the FEM of the elevated water tank prepared with the help of this toolbox (Table 3). The number of finite element nodes on the reservoir walls is 2199. The mass and stiffness matrices of the load carrying system can be used in static, modal and time history analysis. The behavior of the RC material is assumed to be linear. Solid tetrahedral elements are used for the FEM (Fig. 5).

Table 3 Finite element properties of RC elevated water tank

Nodes	Elements	Maximum element size (m)	Minimum element size (m)	Mesh gradation	Geometric order
11682	44204	1.4993	0.7496	1.5	Linear

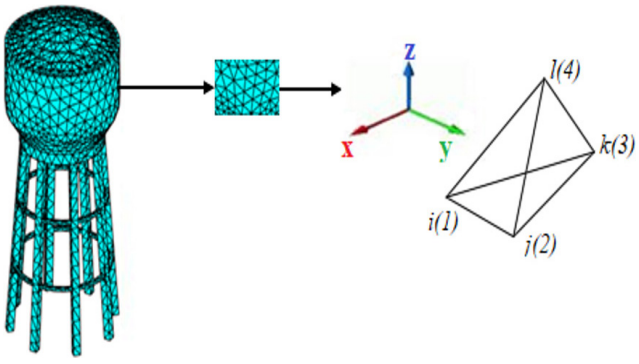

Fig. 5 Solid tetrahedral finite element

Fig. 6 shows the photo of the RC elevated water tank, the mathematical model and the FEM. It can be clearly seen from Fig. 6 that a cylinder and a truncated cone, eight pillars and two pillow beams are utilized in the load carrying system of the cited tank. Also, the cited elevated water tank is assumed to be fixed to the ground. DualSPHysics program (Fig. 7) dependent on the SPH method is used to analyze the cited tank at 50% full and 100% full water levels under cited earthquake acceleration records.

3.3 Modeling water with SPH method

In this study, the nonlinear behavior of the water in the cited elevated tank is considered with the SPH method depending on the Lagrangian approach. In SPH model, the fluid is considered as a particle while solving numerical equations of fluid dynamics and any geometry can be produced that causes this method to be preferred in many areas today. With the determination of an interpolation function (Kernel function), various particle clusters are

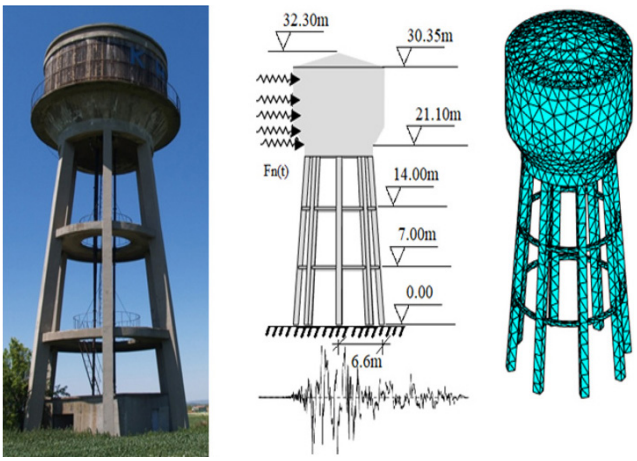

(a) (b) (c)

Fig. 6 Considered RC elevated water tank; (a) Real structure (b) mathematical model and (c) FEM of tank [39]

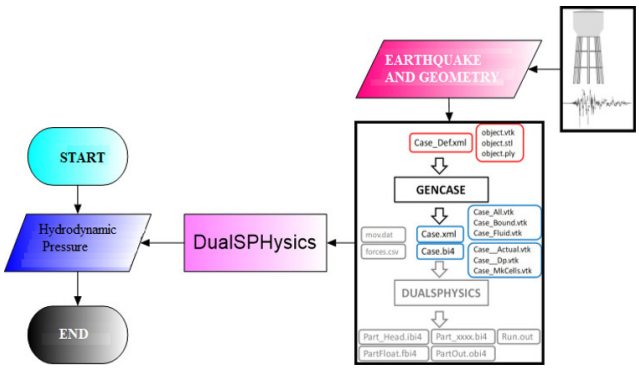

Fig. 7 Flow-chart of DualSPHysics program [15, 39]

arranged [41].

By using SPH method, the ground motion induced water pressures acting on the reservoir walls can be calculated. The DualSphysics program [15], dependent on SPH method, is utilized to obtain hydrodynamic pressures on the reservoir walls. DualSphysics program uses the computer's Central Processing Unit (CPU) and Graphics Processing Unit (GPU) while performing structural analysis. Because of the reason that the number of particles is large and hard to visualize structural analysis' results, working on GPU is preferred in terms of time. To perform the structural seismic analysis, a solid model of the load carrying system of the cited 1000 m^3 RC elevated water tank is produced by using MATLAB PDE toolbox and finite element meshing is applied. After meshing, structural analysis is performed by considering the half and full-filled state of the tank (Table 4) in the DualSphysics program [15]. In seismic analyses, the water level at 50% full and 100% filled level was analyzed according to cited earthquake acceleration records in the DualSPHysics program (using SPH method) (Fig. 8) [39, 42].

Table 4 shows the analysis parameters required for the RC elevated water tank to be 50% and 100% full. For the RC elevated water tank to be 50% and 100% full, the free surface elevation is 25.73 m and 30.35 m, the water height is 4.63 m and 9.25 m, and the water volume is 528.41 m^3 and 1000 m^3, respectively.

Table 4 Parameters of the SPH method for half and full-filled tank [39, 42]

	Half-filled (50%)	Full-filled (100%)
Property	Options	Options
Version	DualSPHysics v4.056	DualSPHysics v4.056
Dimension	3D	3D
Type of the kernel function	Wendland	Wendland
Time-stepping	Verlet	Verlet
Density filter	Shepard filter	Shepard filter
Viscosity treatment	Artificial viscosity (α = 0.01)	Artificial viscosity (α = 0.01)
Boundary conditions (BC)	Dynamic	Dynamic
Distance between particle (dp)	0.09 m	0.20 m
Smoothing length	1	1
The number of fluid particles	38029	95333
Density of water	1000 kg/m^3	1000 kg/m^3
CFL coefficient	0.20	0.20

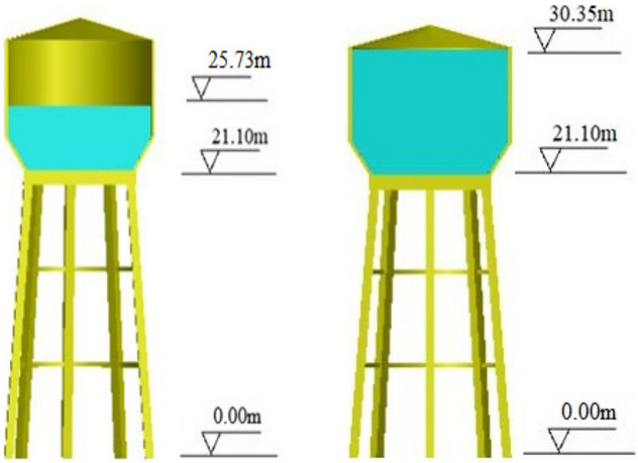

(a) (b)

Fig. 8 Water levels of considered tank; (a) tank is half full (b) tank is full [39, 42]

3.4 Verification of the developed software and FEM model

Within the scope of this study, the validation of the software developed in the MATLAB programming language was carried out using the dynamic analysis results of the floor frame in Chopra [37]. In Fig. 9, smooth and unstarred lines are from Chopra [37], while those with dashed and starred lines are within the scope of this study. By comparison, it was seen that the same values were achieved and verified for the five-degree-of-freedom system.

In the second verification, the free vibration analysis results of the cited elevated water tank were compared with the results in the ANSYS [22] software. It can be seen from Table 5 that the results are close to each other with less than 5% error which can be accepted as the produced model is suitable for the structural analysis [43]. In addition, in accordance with the technical literature, the mode shapes are displacement in the x direction of the 1st mode, displacement in the *y* direction of the 2nd mode and torsion in the 3rd mode shown in Fig. 10.

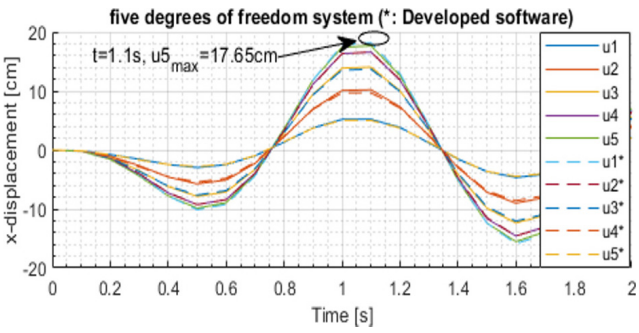

Fig. 9 Comparison of time-dependent variation of displacement of a five-degree-of-freedom system [39]

Table 5 Verification and results of free vibration analysis of empty tank

Case	Mode number	Modal frequency (Hz) (This study-MATLAB)	Modal frequency (Hz) (ANSYS)	Difference (%)	<5%
Empty	1	1.0677	1.0420	2.46	✓
	2	1.0784	1.0497	2.73	✓
	3	1.3288	1.2808	3.74	✓

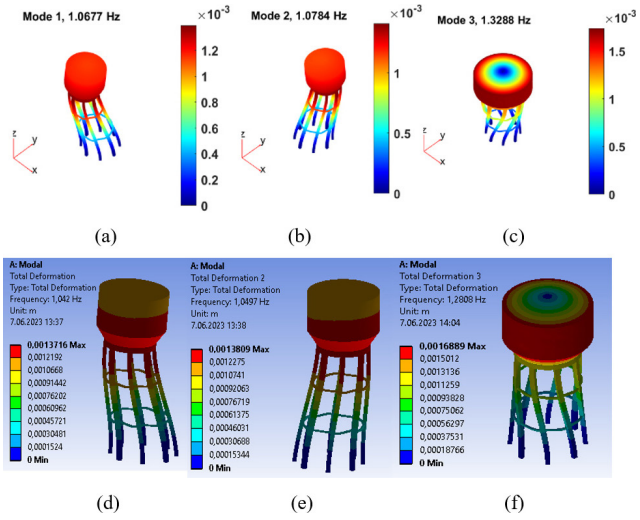

Fig. 10 Results of free vibration analysis; (a) Mode 1; (b) Mode 2; (c) Mode 3 (a,b,c Developed software); (d) Mode 1; (e) Mode 2; (f) Mode 3 (d,e,f ANSYS) [22] (Verification of the developed software)

Moreover, in Table 6, for half-filled and full-filled cases, the first six mode frequencies of the cited elevated water tank is provided. As can be clearly seen from Table 6 that the first three modes of both cases of the cited tank is related with the convective modes of sloshing water.

Table 6 Free vibration analyses of half-filled and full-filled cases of elevated water tank

Case	Mode number	Mode type	Modal frequency (Hz)
Half-filled	1	Convective	0.0182
	2	Convective	0.0183
	3	Convective	0.0247
	4	Translational	0.170
	5	Translational	0.171
	6	Translational	0.217
Full-filled	1	Convective	0.6198
	2	Convective	0.6245
	3	Convective	0.8160
	4	Translational	4.2152
	5	Translational	4.2242
	6	Translational	4.8247

3.5 Time history analysis

For the seismic analysis of the RC elevated water tank, linear time history analyzes were performed. The dynamic condensation method was applied for linear analysis and the solution was obtained with the state-space model at each time step. The Runge-Kutta method was used in the numerical solution of the equations of motion. Rayleigh damping constants were calculated between the first horizontal mode and the sixth mode of the elevated water tank, assuming a 5% damping ratio. Alpha and Beta coefficients were calculated as 0.7441 and 0.0034, respectively. Within the scope of this study, the selected earthquakes whose information provided in Table 7 are used for earthquake ground motion. Also, in Fig. 11 [44], the time histories of cited earthquakes are represented.

4 Results and discussion

Three models were determined for the linear analysis of the RC elevated water tank in the time history analyses. In the first model, the cited RC elevated water tank is empty. In the second model, finite element method and the Westergaard approach (one of the added mass approaches) was used in the load carrying system and for the fluid-structure interaction, respectively. In the third model, the load carrying system is again modeled with the finite element method, and the fluid-structure interaction is modeled with the SPH method (Table 8). Also, the models are named as accordingly. For example, the name of the second model with Westergaard approach and half-full is "Model-2-50-wes". The other models are named as the same way.

4.1 Kocaeli earthquake

As a result of the Kocaeli earthquake analyzes carried out, all hydrodynamic pressures at the finite element nodes of the tank wall were obtained nonlinearly using the SPH method. As an example, the time dependent hydrodynamic pressure variation of a point at the bottom of the tank at the coordinates X = 5.8814 m, Y = 11.396 m, Z = 21.1 m is given in Figs. 12 and 13 for half and full-filled situations, respectively. In this way, nonlinear pressures can be obtained at all points of the cited elevated water tank. However, considering the volume of the study, time-dependent nonlinear hydrodynamic pressure variation is shown for only one point as an example.

When the greatest ground acceleration occurs in 9.87 s, in Fig. 12 and in Fig. 13, the hydrodynamic pressure is 0.59 kPa and 9.29 kPa, respectively. Also, in empty case,

Table 7 Details of the selected ground motions

Number	Record	Year	Component	Station	PGA (g)	PGV (cm/s)	PGD (cm)	Duration (sec)	Closest to fault rupture (km)	M_w
1	Kocaeli (Türkiye)	1999	KOERI330	Yarımca	0.349	62.18	51.3	34.94	3.3	7.4
2	Van (Türkiye)	2011	NE	Muradiye	0.203	33.83	7.44	107.12	11.57	7.2
3	Kahramanmaraş (Türkiye)	2023	EW	Pazarcık	2.198	54.58	18.30	99.33	8.6	7.7
4	Kobe (Japan)	1995	CUE90	Kakogawa	0.345	27.67	9.7	40.88	13.3	7.2

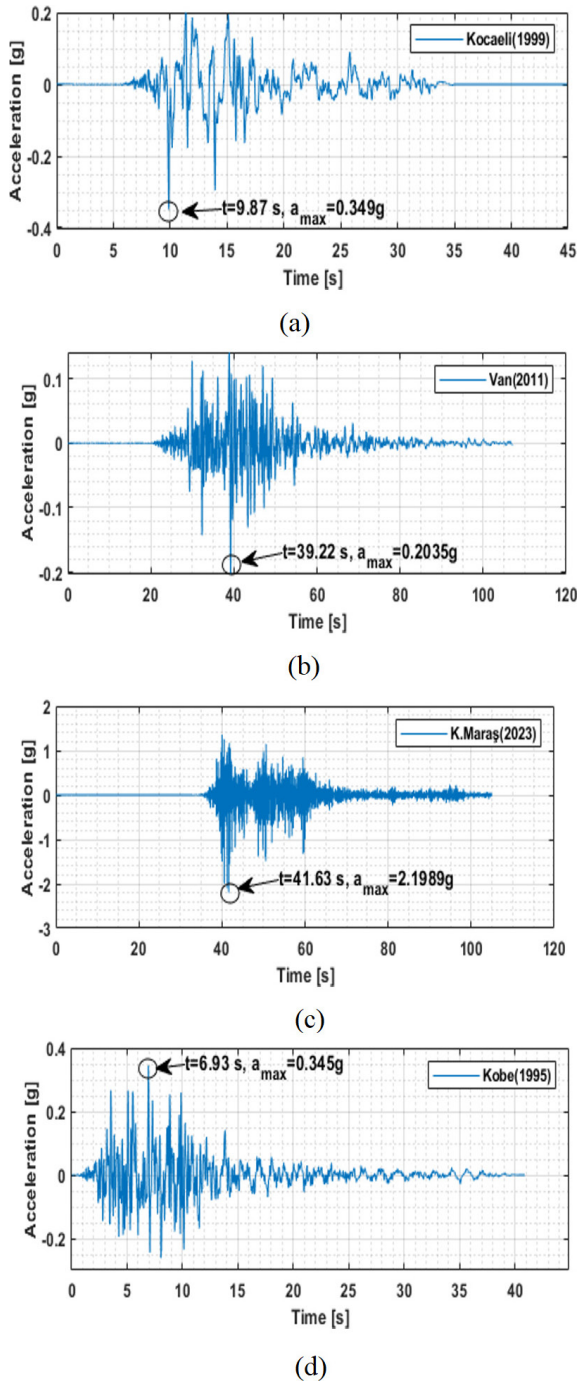

Fig. 11 Time histories of selected earthquakes; (a) Kocaeli earthquake (YPT330); (b) Van earthquake (Muradiye N-S); (c) KahramanMaraş earthquake (4614 E-W); (d) Kobe earthquake (Kakogawa(CUE90)) [44]

Table 8 Models of analysis

	Approach	1. Empty case	Half-filled case (50%)	Full-filled case (100%)
Model-1-emp	–	ok	–	–
Model-2-50-wes	Westergaard	–	ok	–
Model-2-100-wes	Westergaard	–	–	ok
Model-3-50-sph	SPH	–	ok	–
Model-3-100-sph	SPH	–	–	ok

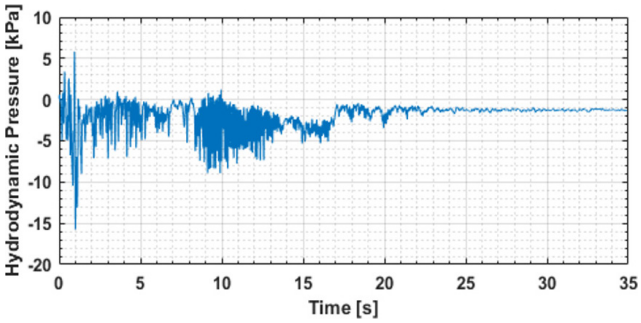

Fig. 12 Hydrodynamic pressure variation at the coordinates $X = 5.8814$ m, $Y = 11.396$ m, $Z = 21.1$ m for half-filled case as an example [39, 42]

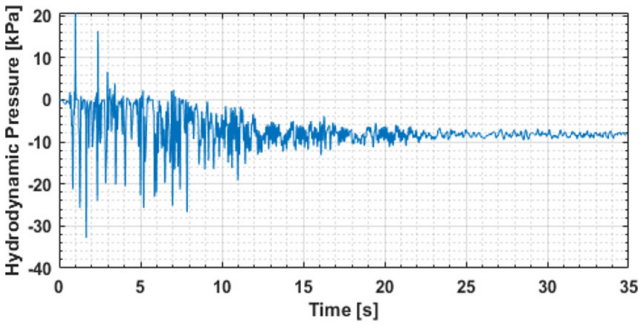

Fig. 13 Hydrodynamic pressure variation at the coordinates $X = 5.8814$ m, $Y = 11.396$ m, $Z = 21.1$ m for full-filled case as an example [39, 42]

for Model-1-emp, change of time dependent displacement in x direction, greatest displacement in x direction and greatest Drucker-Prager (D-P) equivalent stress are provided in Fig. 14, and Fig. 15 (a) and (b), respectively.

In half-filled case, for Model-2-50-wes, change of time dependent displacement in x direction, greatest displacement

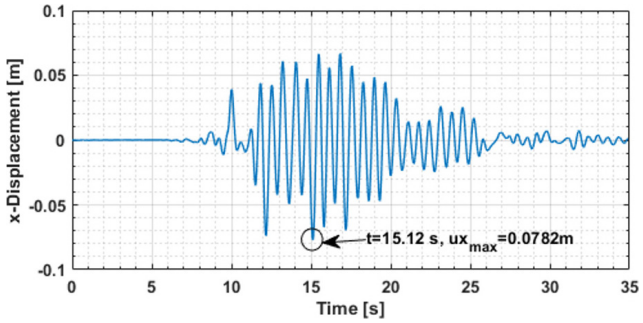

Fig. 14 Time dependent variation of the displacement in the x direction (tank is empty)

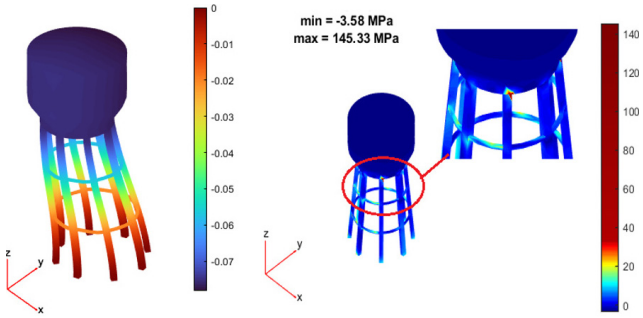

Fig. 15 Analyzed RC water tank under Kocaeli earthquake; (a) greatest displacement in x direction; (b) greatest D-P equivalent stress (tank is empty)

in *x* direction and greatest D-P equivalent stress are provided in Fig. 16, and Fig. 17 (a) and (b), respectively.

In full-filled case, for Model-2-100-wes, change of time dependent displacement in x direction, greatest displacement in x direction and greatest D-P equivalent stress are provided in Figs. 18, and Fig. 19 (a) and (b), respectively.

Considering the results found by using SPH method, in half-filled case, for Model-3-50-sph, change of time dependent displacement in x direction, greatest displacement in x direction and greatest D-P equivalent stress are provided in Fig. 20, and Fig. 21 (a) and (b), respectively.

In full-filled case, for Model-3-100-sph, change of time dependent displacement in x direction, greatest displacement in x direction and greatest D-P equivalent stress are provided in Fig. 22, and Fig. 23 (a) and (b), respectively.

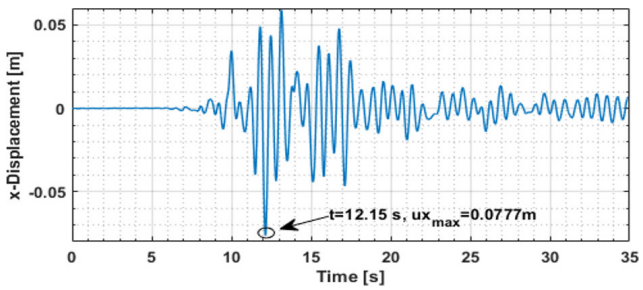

Fig. 16 Time dependent variation of the displacement in the x direction (tank is half-filled)

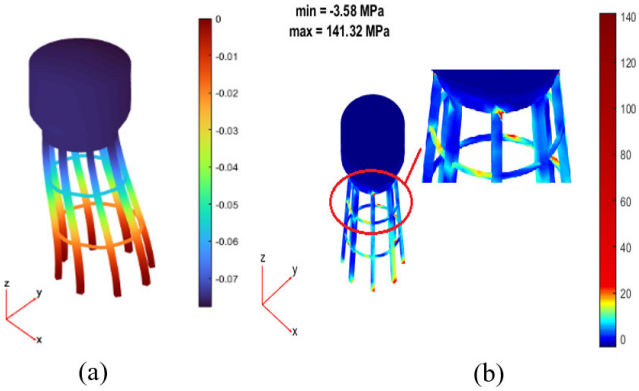

Fig. 17 Analyzed RC water tank under Kocaeli earthquake; (a) greatest displacement in x direction (b) greatest D-P equivalent stress (tank is half-filled)

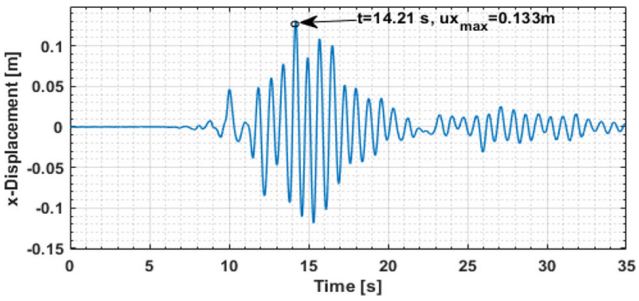

Fig. 18 Time dependent variation of the displacement in the x direction (tank is full-filled)

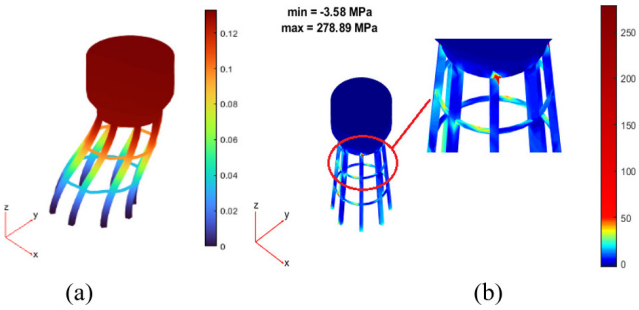

Fig. 19 Analyzed RC water tank under Kocaeli earthquake; (a) greatest displacement in x direction; (b) greatest D-P equivalent stress (tank is full-filled)

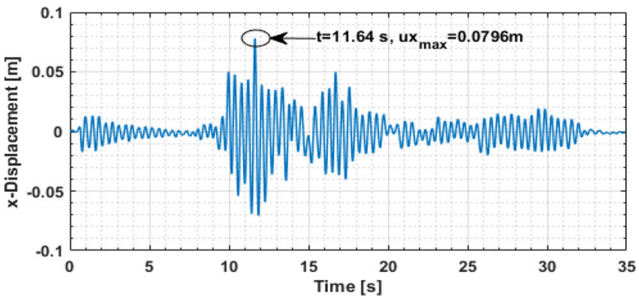

Fig. 20 Time dependent variation of the displacement in the x direction (tank is half-filled)

4.2 Van earthquake

For Van earthquake, the time dependent hydrodynamic pressure variation of points at the bottom of the half and full-filled situations are given in Figs. 24 and 25, respectively.

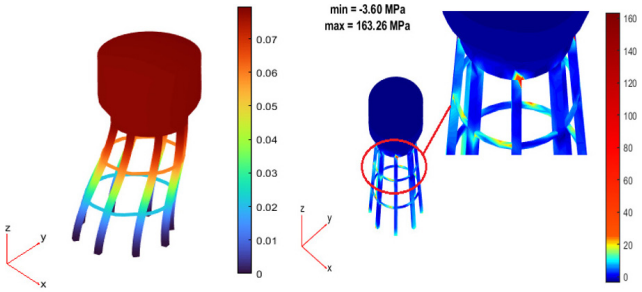

Fig. 21 Analyzed RC water tank under Kocaeli earthquake; (a) greatest displacement in x direction; (b) greatest D-P equivalent stress (tank is half-filled)

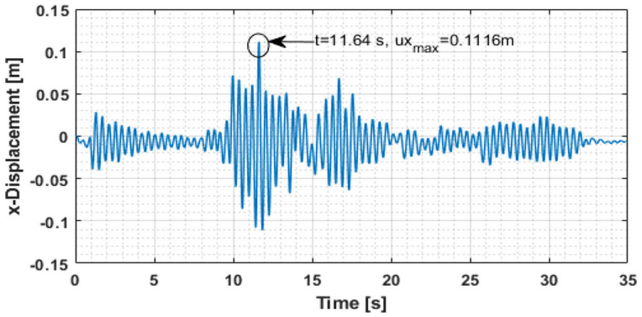

Fig. 22 Time dependent variation of the displacement in the x direction (tank is full-filled)

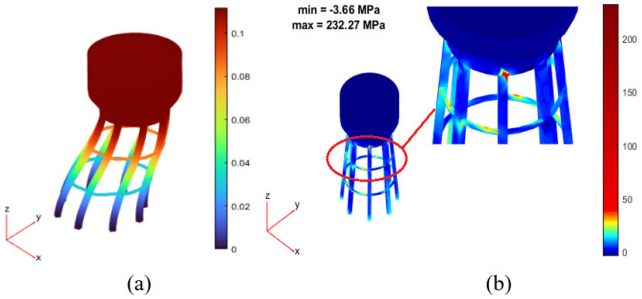

Fig. 23 Analyzed RC water tank under Kocaeli earthquake; (a) greatest displacement in x direction; (b) greatest D-P equivalent stress (tank is full-filled)

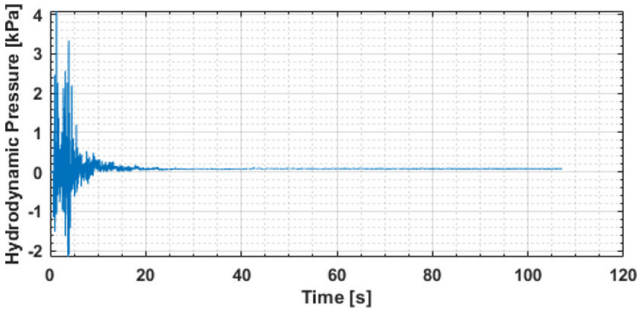

Fig. 24 Hydrodynamic pressure variation at the coordinates $X = 4.19$ m, $Y = 2.77$ m, $Z = 21.1$ m for half-filled case as an example

The greatest ground acceleration occurs in 1.33 s for half-filled case and the hydrodynamic pressure is 4.09 kPa. For full-filled case, the greatest ground acceleration occurs in 2.48 s for full-filled case and the hydrodynamic pressure is 18.76 kPa.

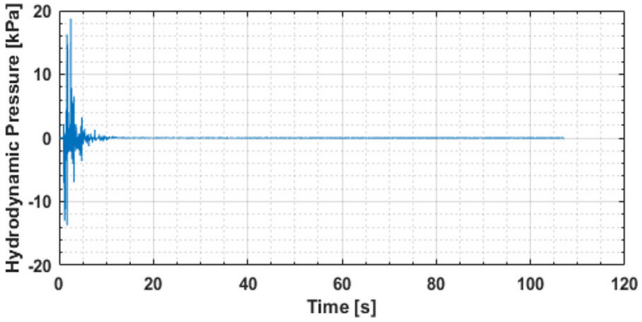

Fig. 25 Hydrodynamic pressure variation at the coordinates $X = 3.48$ m, $Y = 6.34$ m, $Z = 21.1$ m for full-filled case as an example

Also, in empty case, for Model-1-emp, change of time dependent displacement in x direction, greatest displacement in x direction and greatest D-P equivalent stress are provided in Figs. 26, and Fig. 27 (a) and (b), respectively.

In half-filled case, for Model-2-50-wes, change of time dependent displacement in x direction, greatest displacement in x direction and greatest D-P equivalent stress are provided in Fig. 28, and Fig. 29 (a) and (b), respectively.

In full-filled case, for Model-2-100-wes, change of time dependent displacement in x direction, greatest displacement in x direction and greatest D-P equivalent stress are provided in Fig. 30, and Fig. 31 (a) and (b), respectively.

Considering the results found by using SPH method, in half-filled case, for Model-3-50-sph, change of time dependent displacement in x direction, greatest displacement in

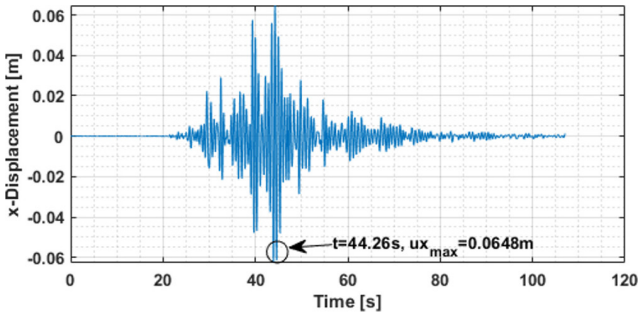

Fig. 26 Time dependent variation of the displacement in the x direction (tank is empty)

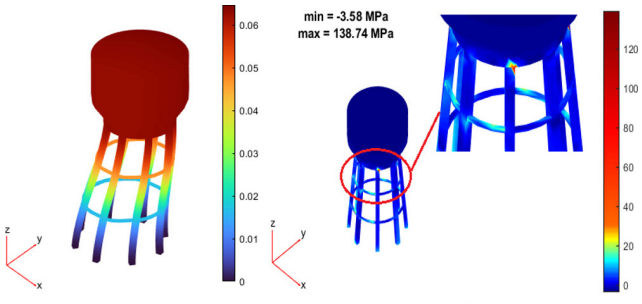

Fig. 27 Analyzed RC water tank under Van earthquake; (a) greatest displacement in x direction; (b) greatest D-P equivalent stress (tank is empty)

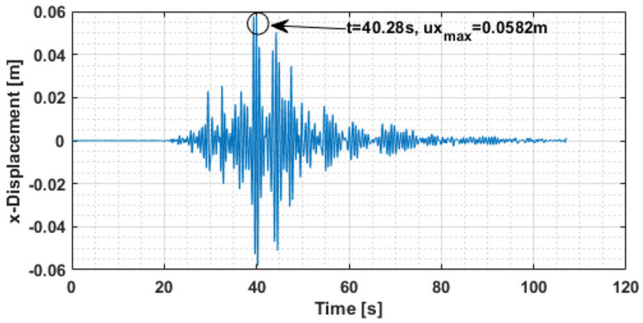

Fig. 28 Time dependent variation of the displacement in the x direction (tank is half-filled)

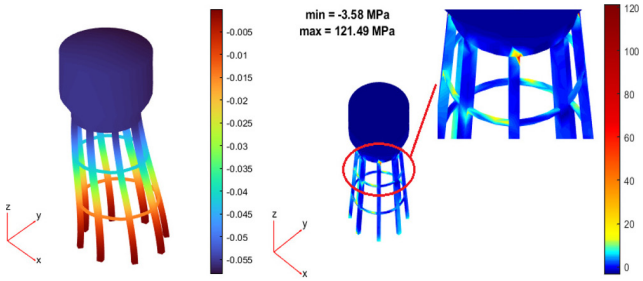

Fig. 29 Analyzed RC water tank under Van earthquake; (a) greatest displacement in x direction; (b) greatest D-P equivalent stress (tank is half-filled)

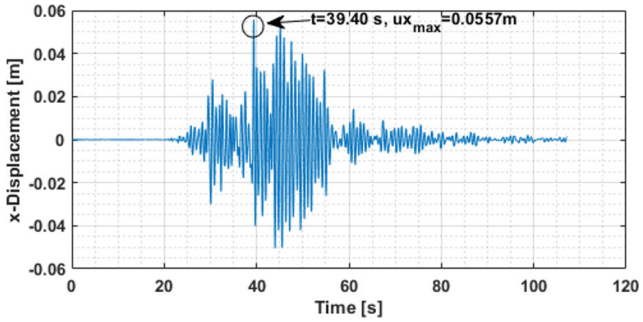

Fig. 30 Time dependent variation of the displacement in the x direction (tank is full-filled)

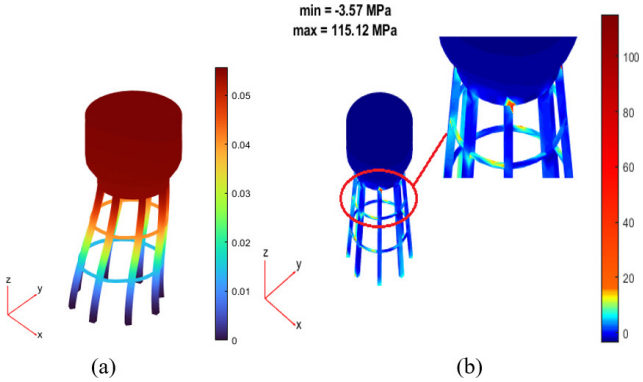

Fig. 31 Analyzed RC water tank under Van earthquake; (a) greatest displacement in x direction; (b) greatest D-P equivalent stress (tank is full-filled)

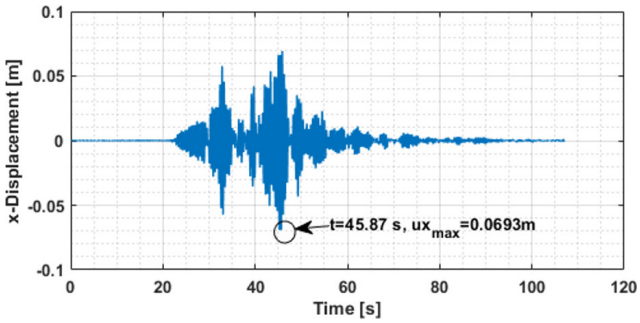

Fig. 32 Time dependent variation of the displacement in the x direction (tank is half-filled)

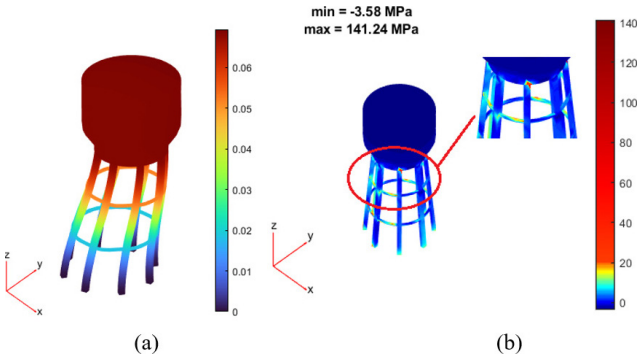

Fig. 33 Analyzed RC water tank under Van earthquake; (a) greatest displacement in x direction; (b) greatest D-P equivalent stress (tank is half-filled)

x direction and greatest D-P equivalent stress are provided in Fig. 32, and Fig. 33 (a) and (b), respectively.

In full-filled case, for Model-3-100-sph, change of time dependent displacement in x direction, greatest displacement in x direction and greatest D-P equivalent stress are provided in Fig. 34, and Fig. 35 (a) and (b), respectively.

4.3 Kahramanmaraş earthquake

For Kahramanmaraş earthquake, the time dependent hydrodynamic pressure variation of points at the bottom of half and full-filled situations are given in Figs. 36 and 37, respectively.

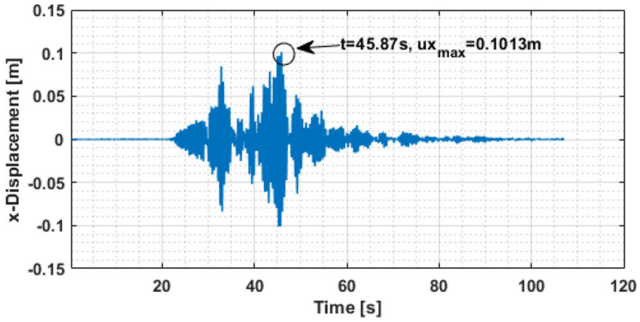

Fig. 34 Time dependent variation of the displacement in the x direction (tank is full-filled)

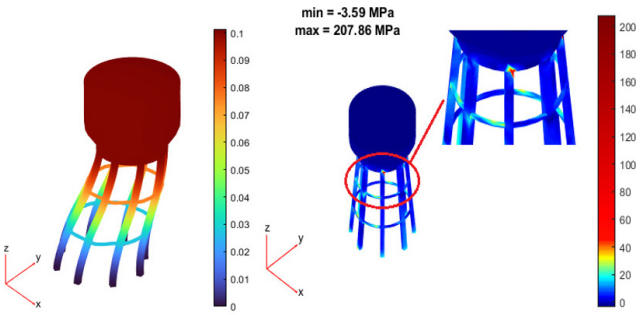

(a) (b)

Fig. 35 Analyzed RC water tank under Van earthquake; (a) greatest displacement in x direction; (b) greatest D-P equivalent stress (tank is full-filled)

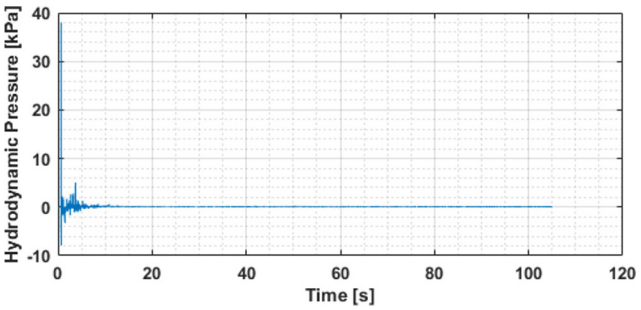

Fig. 36 Hydrodynamic pressure variation at the coordinates $X = 2.69$ m, $Y = 5.38$ m, $Z = 21.1$ m for half-filled case as an example

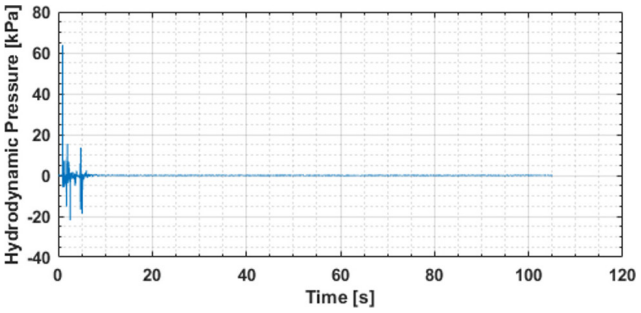

Fig. 37 Hydrodynamic pressure variation at the coordinates $X = 3.58$ m, $Y = 7.93$ m, $Z = 21.1$ m for full-filled case as an example

The greatest ground acceleration occurs in 0.65 s for half-filled case and the hydrodynamic pressure is 37.98 kPa. For full-filled case, the greatest ground acceleration occurs in 0.95 s for full-filled case and the hydrodynamic pressure is 63.82 kPa.

Also, in empty case, for Model-1-emp, change of time dependent displacement in x direction, greatest displacement in x direction and greatest D-P equivalent stress are provided in Fig. 38, and Fig. 39 (a) and (b), respectively.

In half-filled case, for Model-2-50-wes, change of time dependent displacement in x direction, greatest displacement in x direction and greatest D-P equivalent stress are provided in Fig. 40, and Fig. 41 (a) and (b), respectively.

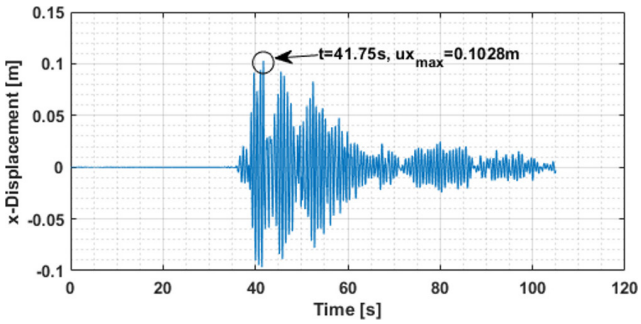

Fig. 38 Time dependent variation of the displacement in the x direction (tank is empty)

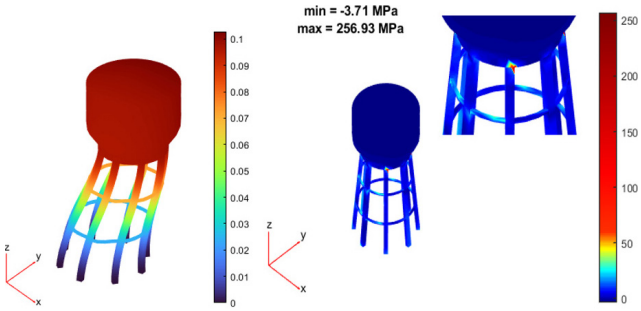

(a) (b)

Fig. 39 Analyzed RC water tank under Kahramanmaraş earthquake; (a) greatest displacement in x direction; (b) greatest D-P equivalent stress (tank is empty)

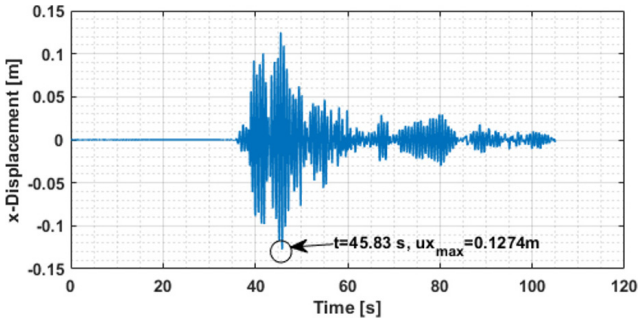

Fig. 40 Time dependent variation of the displacement in the x direction (tank is half-filled)

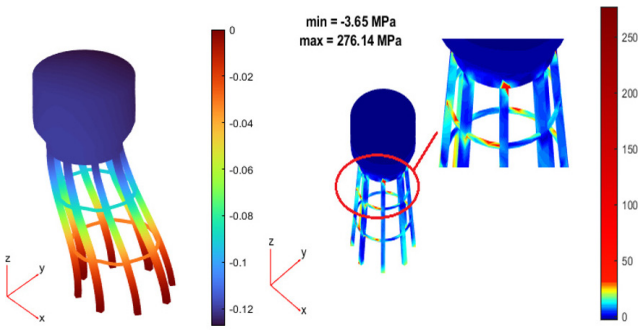

(a) (b)

Fig. 41 Analyzed RC water tank under Kahramanmaraş earthquake; (a) greatest displacement in x direction; (b) greatest D-P equivalent stress (tank is half-filled)

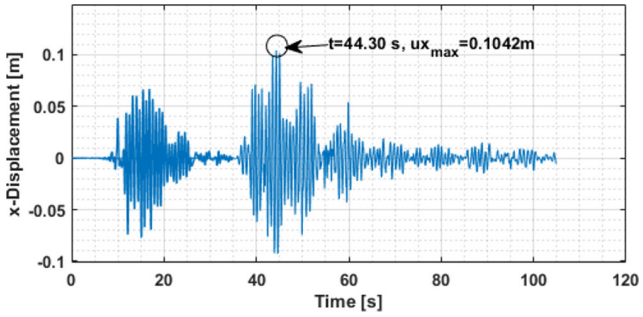

Fig. 42 Time dependent variation of the displacement in the x direction (tank is full-filled)

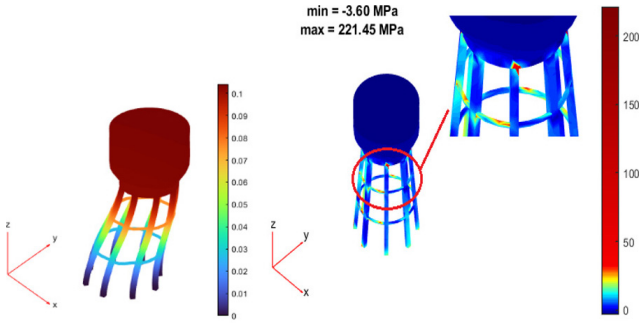

(a) (b)

Fig. 43 Analyzed RC water tank under Kahramanmaraş earthquake; (a) greatest displacement in x direction; (b) greatest D-P equivalent stress (tank is full-filled)

In full-filled case, for Model-2-100-wes, change of time dependent displacement in x direction, greatest displacement in x direction and greatest D-P equivalent stress are provided in Fig. 42, and Fig. 43 (a) and (b), respectively.

Considering the results found by using SPH method, in half-filled case, for Model-3-50-sph, change of time dependent displacement in x direction, greatest displacement in x direction and greatest D-P equivalent stress are provided in Fig. 44, and Fig. 45 (a) and (b), respectively.

In full-filled case, for Model-3-100-sph, change of time dependent displacement in x direction, greatest displacement in x direction and greatest D-P equivalent stress are provided in Fig. 46, and Fig. 47 (a) and (b), respectively.

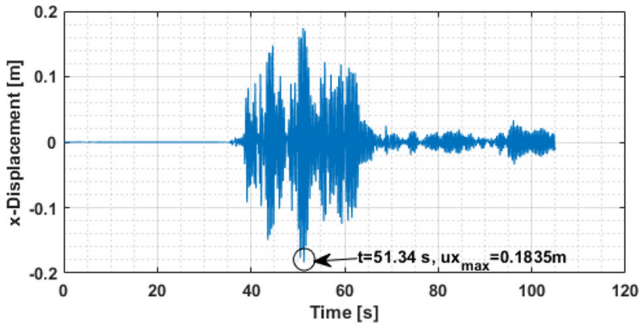

Fig. 44 Time dependent variation of the displacement in the x direction (tank is half-filled)

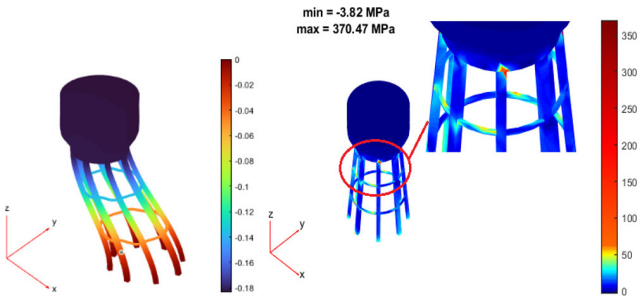

(a) (b)

Fig. 45 Analyzed RC water tank under Kahramanmaraş earthquake; (a) greatest displacement in x direction; (b) greatest D-P equivalent stress (tank is half-filled)

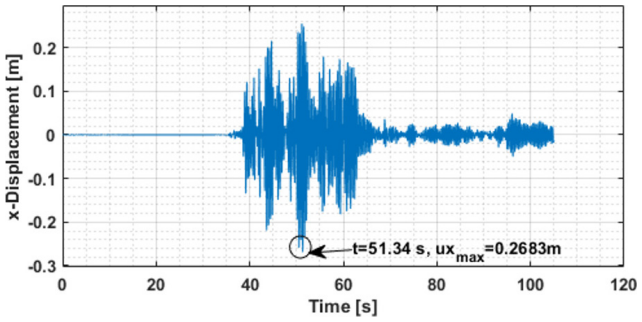

Fig. 46 Time dependent variation of the displacement in the x direction (tank is full-filled)

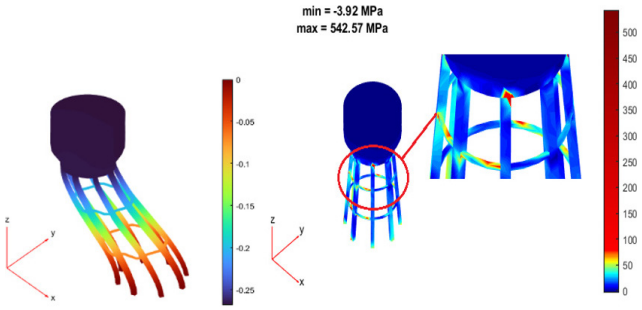

(a) (b)

Fig. 47 Analyzed RC water tank under Kahramanmaraş earthquake; (a) greatest displacement in x direction; (b) greatest D-P equivalent stress (tank is full-filled)

4.4 Kobe earthquake

The time dependent hydrodynamic pressure variation of points at the bottom of the half and full-filled situations are given in Figs. 48 and 49, respectively.

The greatest ground acceleration occurs in 0.68 s for half-filled case and the hydrodynamic pressure is 8.39 kPa. For full-filled case, the greatest ground acceleration occurs in 1.45 s for full-filled case and the hydrodynamic pressure is 28.24 kPa.

Also, in empty case, for Model-1-emp, change of time dependent displacement in x direction, greatest

displacement in x direction and greatest D-P equivalent stress are provided in Fig. 50, and Fig. 51 (a) and (b), respectively.

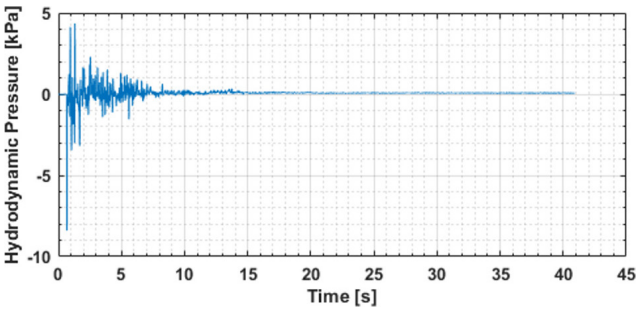

Fig. 48 Hydrodynamic pressure variation at the coordinates $X = 2.82$ m, $Y = 8.42$ m, $Z = 21.1$ m for half-filled case as an example

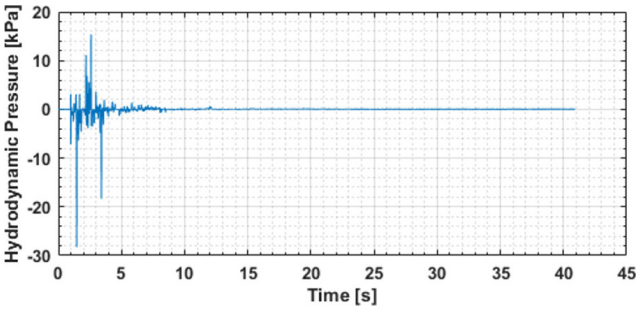

Fig. 49 Hydrodynamic pressure variation at the coordinates $X = 3.36$ m, $Y = 6.87$ m, $Z = 21.1$ m for full-filled case as an example

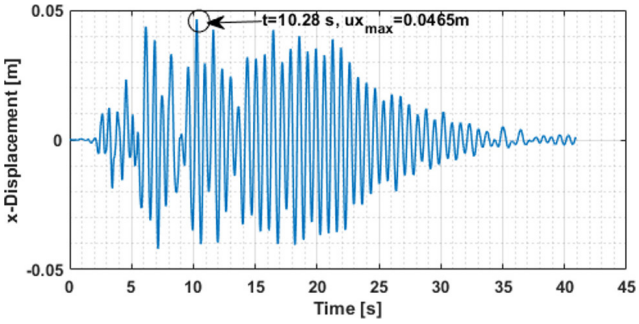

Fig. 50 Time dependent variation of the displacement in the x direction (tank is empty)

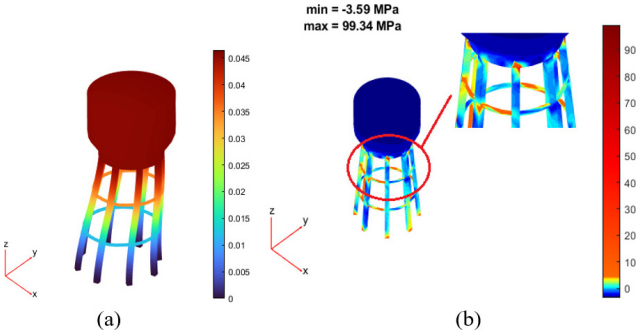

Fig. 51 Analyzed RC water tank under Kobe earthquake; (a) greatest displacement in x direction, (b) greatest D-P equivalent stress (tank is empty)

In half-filled case, for Model-2-50-wes, change of time dependent displacement in x direction, greatest displacement in x direction and greatest D-P equivalent stress are provided in Fig. 52, and Fig. 53 (a) and (b), respectively.

In full-filled case, for Model-2-100-wes, change of time dependent displacement in x direction, greatest displacement in x direction and greatest D-P equivalent stress are provided in Fig. 54, and Fig. 55 (a) and (b), respectively.

Considering the results found by using SPH method, in half-filled case, for Model-3-50-sph, change of time dependent displacement in x direction, greatest displacement in

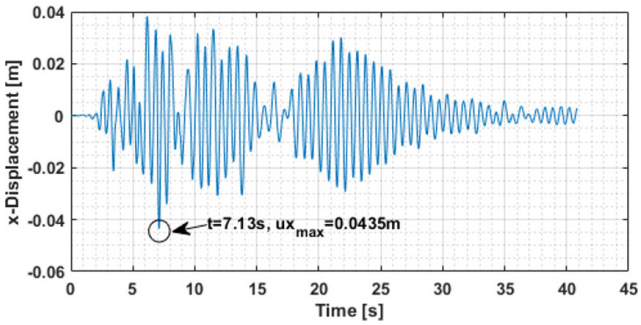

Fig. 52 Time dependent variation of the displacement in the x direction (tank is half-filled)

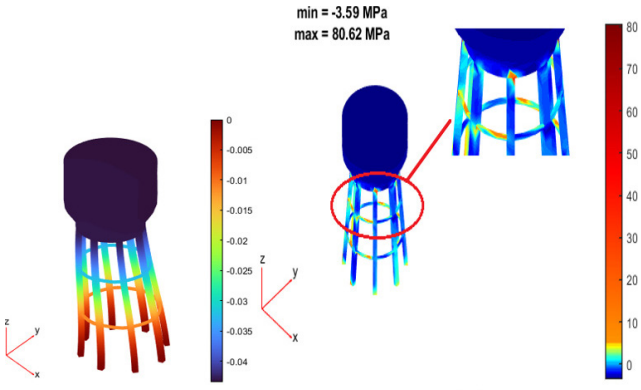

Fig. 53 Analyzed RC water tank under Kobe earthquake; (a) greatest displacement in x direction; (b) greatest D-P equivalent stress (tank is half-filled)

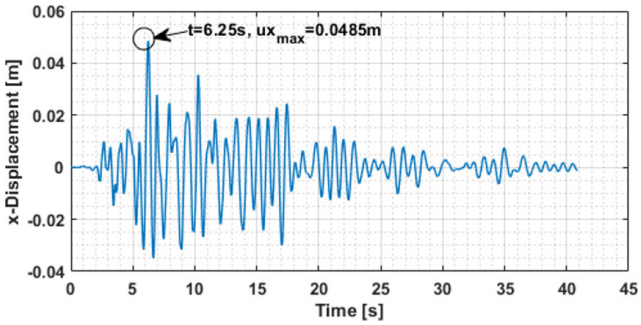

Fig. 54 Time dependent variation of the displacement in the x direction (tank is full-filled)

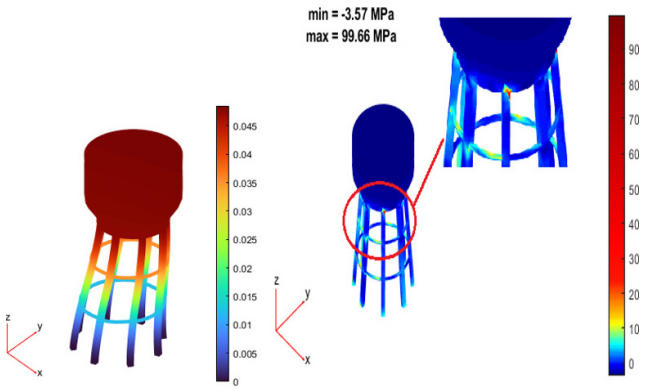

(a) (b)

Fig. 55 Analyzed RC water tank under Kobe earthquake; (a) greatest displacement in x direction; (b) greatest D-P equivalent stress (tank is full-filled)

x direction and greatest D-P equivalent stress are provided in Fig. 56, and Fig. 57 (a) and (b), respectively.

In full-filled case, for Model-3-100-sph, change of time dependent displacement in x direction, greatest displacement in x direction and greatest D-P equivalent stress are provided in Fig. 58, and Fig. 59 (a) and (b), respectively.

In this study, as a result of the structural analyzes of the considered models provided in Table 8 for the cited earthquakes, the Drucker-Prager yield rule (given in the preceding section of this study) is utilized to evaluate whether cracks occurred or not. According to the Drucker-Prager yield rule, only in the Model-3-100-sph (tank is full and SPH method is used) under Kahramanmaraş earthquake, the yield value of the reinforcing steel (420 MPa) is exceeded which shows the probability of cracking to be occurred. From this it is concluded that damage will occur depending on cracks due to the increase in earthquake ground acceleration. Also, for all models considered in Table 8, the compression strength of the concrete (25 MPa) is not exceeded. Moreover, even though the produced software in this study allows three-dimensional analysis (with vertical direction), as in the case in the technical literature, two-dimensional structural analysis was preferred.

The results given in the preceding figures are totally provided in Table 9 for comparison purpose. Also, the values represented in Table 9 are provided in Figs. 60–63 separately for the cited earthquakes.

The interpretation of Table 9 and Figs. 60–63 revealed that both for half-filled and full-filled cases, Kahramanmaraş earthquake created the maximum demands (x-displacements and D-P equivalent stresses) among other earthquakes that is considered. In this earthquake, it can be clearly seen that for the Westergaard approach and SPH

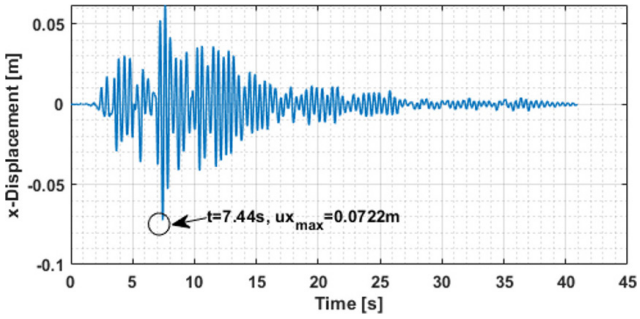

Fig. 56 Time dependent variation of the displacement in the x direction (tank is half-filled)

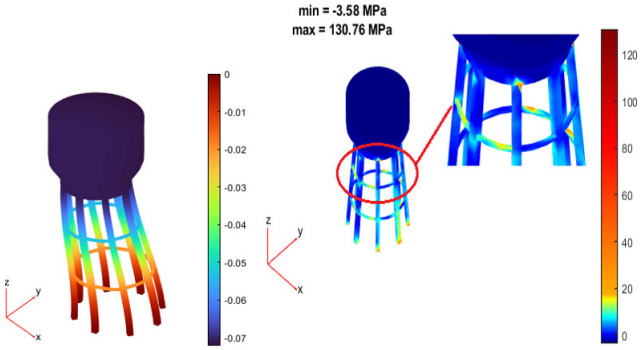

(a) (b)

Fig. 57 Analyzed RC water tank under Kobe earthquake; (a) greatest displacement in x direction; (b) greatest D-P equivalent stress (tank is half-filled)

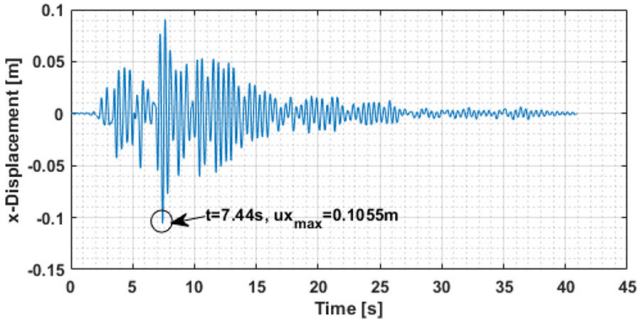

Fig. 58 Time dependent variation of the displacement in the x direction (tank is full-filled)

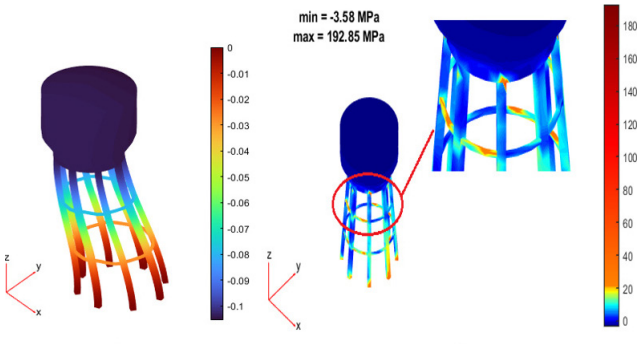

(a) (b)

Fig. 59 Analyzed RC water tank under Kobe earthquake; (a) greatest displacement in x direction; (b) greatest D-P equivalent stress (tank is full-filled)

Table 9 The comparison of analysis results obtained from Westergaard approach and SPH method for half and full-filled RC elevated water tank

Earthquake		Westergaard approach	SPH method	Difference (%)	Westergaard approach	SPH method	Difference (%)
Kocaeli	Percent of Filling (%)	50%	50%	–	100%	100%	–
	Displacement (u_x) (m)	0.0777	0.0796	+2.45	0.133	0.1116	−16.090
	Drucker-Prager (Compression) (Mpa)	−3.58	−3.60	+0.56	−3.58	−3.66	+2.23
	Drucker-Prager (Tension) (Mpa)	+141.32	+163.26	+15.53	+278.89	+232.27	−16.72
Van	Displacement (u_x) (m)	0.0582	0.0693	+19.07	0.0557	0.1013	+81.86
	Drucker-Prager (Compression) (Mpa)	−3.58	−3.58	0	−3.57	−3.59	+0.56
	Drucker-Prager (Tension) (Mpa)	+121.49	+141.24	+16.26	+115.12	+207.86	+80.56
Kahramanmaraş	Displacement (u_x) (m)	0.1274	0.1835	+44.03	0.1042	0.2683	+157.48
	Drucker-Prager (Compression) (Mpa)	−3.65	−3.82	+4.66	−3.60	−3.92	+8.89
	Drucker-Prager (Tension) (Mpa)	+276.14	+370.47	+34.16	+221.45	+542.57	+145.01
Kobe	Displacement (u_x) (m)	0.0435	0.0722	+65.97	0.0485	0.1055	+117.52
	Drucker-Prager (Compression) (Mpa)	−3.59	−3.58	−0.28	−3.57	−3.58	+0.28
	Drucker-Prager (Tension) (Mpa)	+80.62	+130.76	+62.19	+99.66	+192.85	+93.50

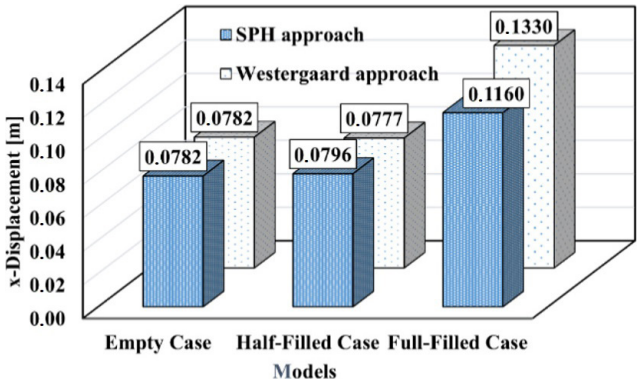

Fig. 60 x-direction displacements of Westergaard approach and SPH method for both half and full-filled case (Kocaeli)

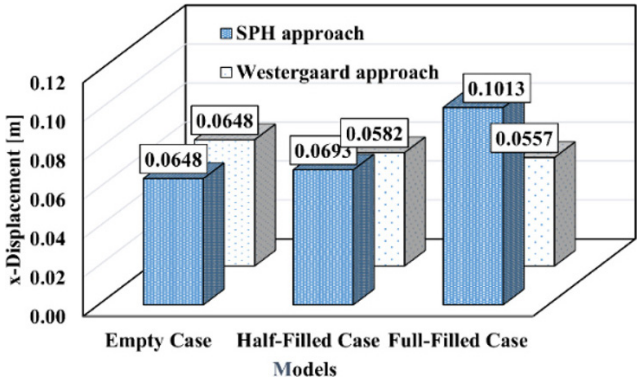

Fig. 61 x-direction displacements of Westergaard approach and SPH method for both half and full-filled case (Van)

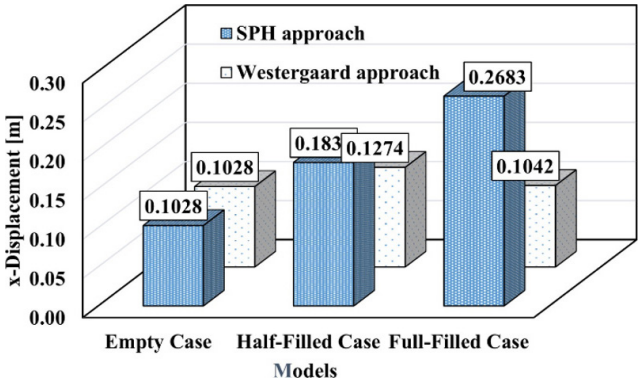

Fig. 62 x-direction displacements of Westergaard approach and SPH method for both half and full-filled case (Kahramanmaraş)

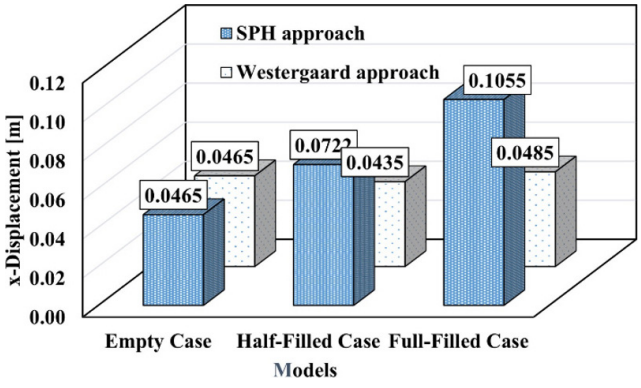

Fig. 63 x-direction displacements of Westergaard approach and SPH method for both half and full-filled case (Kobe)

method, there is a +44.03% and 157.48% difference between the largest displacements in the x direction in case the tank is half-filled and full-filled, respectively. In the same manner (Kahramanmaraş earthquake), for the Westergaard approach and SPH method, there is a +34.16% and +145.01% difference (in tension stress) in the D-P equivalent stresses in case the tank is half-filled and full-filled, respectively. Moreover, for compression stress, in Westergaard approach and SPH method, there is a +4.66% and +8.89% difference in the D-P equivalent stresses in case the tank is half-filled and full-filled, respectively. From the findings of this study, it is seen that D-P equivalent stresses (tension), increase mostly at the lower and upper ends of the column, at the column-beam junctions, and in the regions where the reservoir and the columns meet. In addition, from Table 9, except for Kahramanmaraş earthquake (full-filled case in SPH), D-P equivalent stress values are well below the yield value $f_y = 420$ MPa of the RC rebar (S420) in all of the analyses. For this reason, in Kahramanmaraş earthquake (full-filled case in SPH), the cited RC elevated water tank has the possibility to be heavily damaged or totally collapsed from the cited regions (shown in the preceding figures). Also, from the interpretation of Table 9, it can be clearly identified that for all models considered, the compression strength of the concrete (25 MPa) is not exceeded.

As it is emphasized in the preceding sections, recent Kahramanmaraş earthquake created maximum demands for the cited RC elevated water tank. Also, in this earthquake, so many RC elevated water tanks are heavily damaged or totally collapsed. One of them is given in Fig. 64 which is heavily damaged in recent Kahramanmaraş earthquake and demolished in controlled manner.

As can be seen from Fig. 64 [45] that the heavily damaged RC elevated water tank is demolished from the column-beam junctions which is consistent with the findings of this study.

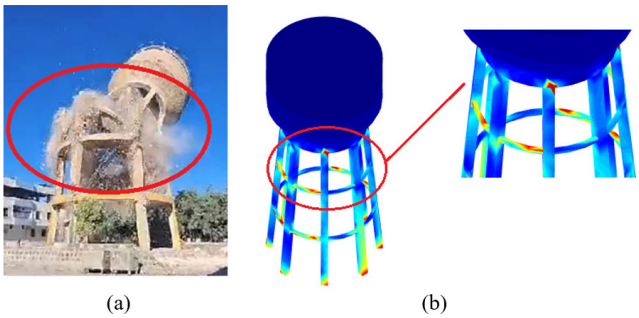

(a) (b)

Fig. 64 Structural earthquake response comparison of (a) a heavily damaged RC elevated water tank in recent Kahramanmaraş earthquake [45]; (b) D-P equivalent stress distribution contours for Kahramanmaraş earthquake

5 Conclusions

In this study, the dynamic behavior of a 1000 m^3 RC elevated water tank under the influence of earthquake ground motions was investigated with Westergaard approach and SPH method that considers fluid-structure interaction. The load carrying system of the cited tank is modeled by the finite element method and the fluid part is modeled by the Westergaard approach and SPH method. In the Westergaard approach, the traditional one, the fluid effect is considered by adding mass to the finite elements in the reservoir walls, and in the SPH method, the hydrodynamic pressures on the reservoir walls due to earthquake accelerations were considered as external forces. Hydrodynamic pressures were obtained for half-filled and full-filled cases with Dualsphysics software based on the SPH method. These pressures were used in the analysis at each time step as an external force in the software developed in the MATLAB programming language. In this software, linear analyzes in time history were performed with ODE45 functions based on Runge-Kutta method by using PDE toolbox functions based on finite element method.

Both the change of hydrodynamic pressures at each time step and the difficulties in dynamic analysis of the finite element (memory, time problems, etc.), dynamic condensation is applied which makes analyzes in the personal computers much easier. The main conclusions that can be deducted from this study is as follows:

- By comparing the displacements for Westergaard approach and SPH method in half-filled case (50%), SPH method provided greater percentage results as +2.45% for Kocaeli, +19.07% for Van, +44.03% for Kahramanmaraş and +65.97% for Kobe earthquakes than traditional Westergaard approach. Although the largest percentage difference for half-filled case between the Westergaard approach and SPH method occurred in Kobe earthquake, the largest displacement is 18.35 cm. in Kahramanmaraş earthquake for SPH method approximately two times of the results obtained in other earthquakes. As can be generalized for half-filled case that SPH method provided much more conservative values compared to Westergaard approach.
- For full-filled case (100%), except for Kocaeli earthquake, SPH method provided positive percentage displacement values when compared with traditional Westergaard approach. The percentage results obtained as −16.09% for Kocaeli, +81.86% for Van, +157.48% for Kahramanmaraş and +117.52% for Kobe earthquake. The largest percentage difference and the largest displacement occurred in recent

Kahramanmaraş earthquake which is +157.48% and 26.83 cm. for SPH method, respectively. This displacement value is approximately larger than two times of the results obtained in other earthquakes. This shows that SPH method gives conservative values when compared to traditional Westergaard approach.

- For D-P equivalent stresses (tension) for Westergaard approach and SPH method in half-filled case (50%), SPH method provided greater percentage results as +15.53% for Kocaeli, +16.26% for Van, +34.16% for Kahramanmaraş and +62.19% for Kobe earthquakes than traditional Westergaard approach. The largest D-P equivalent stresses (tension) stress occurred as 370.47 MPa (which is approximately 2.5 times larger than the results obtained from other earthquakes in this study) for SPH method under Kahramanmaraş earthquake among other earthquakes considered in this study. For half-filled case, SPH method can be considered as more conservative than the traditional Westergaard approach.
- In full-filled case (100%), except for Kocaeli earthquake, SPH method provided positive percentage D-P equivalent stress (tension) values when compared with traditional Westergaard approach. SPH method provided percentage results as −16.72% for Kocaeli, +80.56% for Van, +145.01% for Kahramanmaraş and +93.50% for Kobe earthquakes than traditional Westergaard approach. The largest percentage difference and the largest D-P equivalent stress (tension) occurred in recent Kahramanmaraş earthquake which is +145.01% and 542.57 MPa for SPH method, respectively. Also, for Kahramanmaraş earthquake, D-P equivalent stress (tension) value of 542.57 MPa is exceeding the yield value of f_y = 420 MPa which shows the destruction severity of the earthquake.
- It is evident from the interpretation of the analyses results (D-P equivalent compression stress results) that none of the models taken into consideration exceed the concrete compression strength which is 25 MPa.
- According to the findings of this study, D-P equivalent stresses (tension) are found to increase primarily at the column's lower and upper ends, at the column-beam connections, and in the areas where the columns and reservoir meet. Therefore, extra care should be taken in design (reinforcement) and construction (control of reinforcement and concrete) phase of such critical areas in order to prevent brittle failure without showing any ductile behavior.
- As the Westergaard approach depends on adding liquid mass to the tank wall, the damping of the sloshing water with time cannot be considered in the seismic analysis. However, in SPH method, the sloshing response of the water with time can be considered which is the case in real earthquakes.

As a result of the analysis, it is seen that the fluid-structure interaction method significantly affects the dynamic behavior of the RC elevated water tank. Since the nonlinear behavior of the fluid during the earthquake is modeled at each time step with the SPH method, it is seen that it gives more realistic and conservative results than the Westergaard approach, which is one of the traditional fluid-structure interaction approaches. Although the results in this study belongs to one specific example, the results obtained can be generalized to many situations.

Acknowledgment

This work is supported by the TUBITAK-BIDEB 2211/C PhD Scholarship Program. Moreover, computing resources used in this work were provided by the National Center for High Performance Computing of Turkey (UHeM) under grant number <4010392021>. Upon request, software developed can be provided. The numerical calculations reported in this paper were fully/partially performed at TUBITAK ULAKBIM, High Performance and Grid Computing Center (TRUBA resources).

References

[1] Steinbrugge, K. V., Rodrigo, F. A. "The Chilean earthquakes of May, 1960: A structural engineering viewpoint", Bulletin of the Seismological Society of America, 53(2), pp. 225–307, 1963. https://doi.org/10.1785/BSSA0530020225

[2] Minowa, C. "Dynamic analysis for rectangular water tanks", Recent Advances in Lifeline Earthquake Engineering in Japan, 1980, pp. 447–450, 1980. [online] Available at: https://www.iitk.ac.in/nicee/wcee/article/7_vol5_447.pdf [Accessed: 11 June 2024]

[3] Knoy, E. C. "Performance of Elevated Tanks During Recent California Seismic Events", presented at 1995 AWWA Annual Conference & Exhibition, Anaheim, CA, USA, Jun. 18–22., 1995.

[4] ITU "Depremleri: Nihai Repor" (Kahramanmaraş Earthquakes Final Report), Istanbul Technical University, Istanbul, Türkiye, 2023. [online] Available at: https://haber.itu.edu.tr/docs/default-source/default-document-library/2023_itu_subat_2023_deprem_son_raporu.pdf?sfvrsn=1583fe76_2 (in Turkish)

[5] Haroun, M. A., Ellaithy, H. M. "Seismically Induced Fluid Forces on Elevated Tanks", Journal of Technical Topics in Civil Engineering, 111(1), pp. 1–15, 1985. https://doi.org/10.1061/JTCEDL.0000023

[6] Housner, G. W. "The dynamic behavior of water tanks", Bulletin of the Seismological Society of America, 53(2), pp. 381–387, 1963. https://doi.org/10.1785/BSSA0530020381

[7] Livaoglu, R., Dogangun, A. "Effect of foundation embedment on seismic behavior of elevated tanks considering fluid-structure-soil interaction", Soil Dynamics and Earthquake Engineering, 27(9), pp. 855–863, 2007. https://doi.org/10.1016/j.soildyn.2007.01.008

[8] Dogangun, A., Durmus, A., Ayvaz, Y. "Earthquake analysis of flexible rectangular tanks by using the Lagrangian fluid finite element", European Journal of Mechanics. A, Solids, 16(1), pp. 165–182, 1997. [online] Available at: https://www.osti.gov/etdeweb/biblio/599232 [Accessed: 11 June 2024]

[9] Westergaard, H. M. "Water Pressures on Dams during Earthquakes", Transactions of the American Society of Civil Engineers, 98(2), pp. 418–433, 1933. https://doi.org/10.1061/TACEAT.0004496

[10] Hoskins, L. M., Jacobsen, L. S. "Water pressure in a tank caused by a simulated earthquake", Bulletin of the Seismological Society of America, 24(1), pp. 1–32, 1934. https://doi.org/10.1785/BSSA0240010001

[11] Werner, P. W., Sundquist, K. J. "On hydrodynamic earthquake effects", Eos, Transactions American Geophysical Union, 30(5), pp. 636–657, 1949. https://doi.org/10.1029/TR030i005p00636

[12] Monaghan, J. J. "Smoothed Particle Hydrodynamics", Annual Review of Astronomy Astrophysics, 30, pp. 543–574, 1992. https://doi.org/10.1146/annurev.aa.30.090192.002551

[13] Cossins, P. J. "Smoothed Particle Hydrodynamics", PhD thesis, University of Leicester, 2010.

[14] Trimulyono, A., Hashimoto, H. "Experimental Validation of Smoothed Particle Hydrodynamics on Generation and Propagation of Waterwaves", Journal of Marine Science and Engineering, 7(1), 17, 2019. https://doi.org/10.3390/jmse7010017

[15] DualSPHysics "DualSPHysics", [online] Available at: https://dual.sphysics.org/sphysics-project/ [Accessed: 15 May 2022]

[16] Lakhade, S. O., Kumar, R., Jaiswal, O. R. "Estimation of drift limits for different seismic damage states of RC frame staging in elevated water tanks using Park and Ang damage index", Earthquake Engineering and Engineering Vibration, 19(1), pp. 161–177, 2020. https://doi.org/10.1007/s11803-020-0554-1

[17] Baghban, M. H., Razavi Tosee, S. V., Valerievich, K. A., Najafi, L., Faridmehr, I. "Seismic Analysis of Baffle-Reinforced Elevated Storage Tank Using Finite Element Method", Buildings, 12(5), 549, 2022. https://doi.org/10.3390/buildings12050549

[18] Alemzadeh, H., Shakib, H., Khanmohammadi, M. "Development of Rocking Isolation for Response Mitigation of Elevated Water Tanks under Seismic and Wind Hazards", Shock and Vibration, 2020(1), 5498298, 2020. https://doi.org/10.1155/2020/5498298

[19] Gurkalo, F., He, C., Poutos, K., He, N. "Effects of innovative reinforced concrete slit shaft configuration on seismic performance of elevated water tanks", Scientific Reports, 14(1), 6113, 2024. https://doi.org/10.1038/s41598-024-56851-3

[20] Tavakoli, D., Ahmadi, A. "The Behavior of Elevated Water Tanks under Impact Loading", Periodica Polytechnica Civil Engineering, 65(4), pp. 1061–1071, 2021. https://doi.org/10.3311/PPci.18533

[21] Tiwari, N., Hora, M. "Transient analysis of elevated intze water tank fluid soil system", Journal of Engineering and Applied Sciences, 10, pp. 869–882, 2015.

[22] ANSYS "ANSYS, Swanson Analysis System, US.", [online] Avaible at: https://www.ansys.com/ [Accessed: 11 June 2024]

[23] Jaiprakash Chitte, C., Charhate, S., Sangita Mishra, S. "Seismic performance of R. C. elevated water storage tanks", Materials Today: Proceedings, 65, pp. 901–907, 2022. https://doi.org/10.1016/j.matpr.2022.03.523

[24] Martínez-Martín, F. J., Yepes, V., González-Vidosa, F., Hospitaler, A., Alcalá, J. "Optimization Design of RC Elevated Water Tanks under Seismic Loads", Applied Sciences, 12(11), 5635, 2022. https://doi.org/10.3390/app12115635

[25] Mansour, A. M., Nazri, F. M. "On the Influence of Fluid–Structure Interaction and Seismic Design on Frame-Supported Elevated Water Tanks", Structural Engineering International, 33(1), pp. 17–31, 2023. https://doi.org/10.1080/10168664.2021.1948379

[26] MATLAB "MATLAB", [online] Available at: https://matlab.mathworks.com/ [Accessed: 11 June 2024]

[27] Doğangün, A., Ayvaz, Y., Durmuş, A. "Earthquake behavior of water tanks with different legs", presented at The Turkish Civil Engineering 14th Technical Congress, Istanbul, Türkiye, Sept. 1–4., 1997.

[28] Monaghan, J. J. "Simulating Free Surface Flows with SPH", Journal of Computational Physics, 110(2), pp. 399–406, 1994. https://doi.org/10.1006/jcph.1994.1034

[29] Lucy, L. B. "A numerical approach to the testing of the fission hypothesis", Astronomical Journal, 82, pp. 1013–1024, 1977. https://doi.org/10.1086/112164

[30] Gingold, R. A., Monaghan, J. J. "Smoothed particle hydrodynamics: theory and application to non-spherical stars", Monthly Notices of the Royal Astronomical Society, 181(3), pp. 375–389, 1977. https://doi.org/10.1093/mnras/181.3.375

[31] Liu, G. R., Liu, M. B. "Smoothed Particle Hydrodynamics: A Meshfree Particle Method", World Scientific, 2003. ISBN 9789812564405 https://doi.org/10.1142/5340

[32] Chen, W.-F., Han, D.-J. "Plasticity for structural engineers", J. Ross publishing, 2007. ISBN 978-1932159752

[33] Paz, M. "Dynamic Condensation", AIAA Journal, 22(5), pp. 724–727, 1984. https://doi.org/10.2514/3.48498

[34] Gavin, H. P. "Model Condensation: CEE 541. Structural Dynamics", [pdf] Department of Civil and Environmental Engineering, Duke University, Durham, NC, USA, 2016. Available at: https://people.duke.edu/~hpgavin/StructuralDynamics/ModelCondensation.pdf [Accessed: 11 June 2024]

[35] Tehrani, M. H., Harvey Jr., P. S., Gavin, H. P., Mirza, A. M. "Inelastic condensed dynamic models for estimating seismic demands for buildings", Engineering Structures, 177, pp. 616–629, 2018. https://doi.org/10.1016/j.engstruct.2018.07.083

[36] Paz, M., Leigh, W. E. "Structural Dynamics: Theory and Computation", Springer, 2004. ISBN 1-4020-7667-3

[37] Chopra, A. K. "Dynamics of Structures", Pearson Education, 2007. ISBN 9780273774242

[38] Livaoglu, R. "Soil interaction effects on sloshing response of the elevated tanks", Geomechanics and Engineering, 5(4), pp. 283–297, 2013. https://doi.org/10.12989/gae.2013.5.4.283

[39] Köksal, O. "Nonlinear Analysis of Reinforced Concrete Elevated Water Tanks Under Various Interactions with Computer Software to Be Created", PhD thesis, Ondokuz Mayıs University, 2023.

[40] Doğangün, A. "Betonarme Yapıların Hesap ve Tasarımı" (Calculation and Design of Reinforced Concrete Structures), Birsen Yayinevi, 2020. ISBN 9789755113104 (in Turkish)

[41] Wendland, H. "Piecewise polynomial, positive definite and compactly supported radial functions of minimal degree", Advances in Computational Mathematics, 4(1), pp. 389–396, 1995. https://doi.org/10.1007/BF02123482

[42] Köksal, O., Karaca, Z., Türkeli, E. "Nonlinear Sloshing Response of Liquid-Filled Reinforced Concrete (RC) Elevated Water Tank Under Seismic Excitation", In: Tasdemir, S., Ozkan, I, A. (eds.) Innovations and Technologies in Engineering, Eğitim Yayınevi, 2022, pp. 268–278. E-ISBN 978-625-6382-83-1

[43] Shakib, H., Alemzadeh, H. "The effect of earthquake site-source distance on dynamic response of concrete elevated water tanks", Procedia Engineering, 199, pp. 260–265, 2017. https://doi.org/10.1016/j.proeng.2017.09.020

[44] PEER "Pacific Earthquake Engineering Research Center", [online] Available at: https://peer.berkeley.edu/ [Accessed: 11 June 2024]

[45] Ajans Urfa Topluluk Kuralları'nı "Urfa'da depremde hasar gören su kulesi kontrollü yıkıldı" (The water tower damaged in the earthquake in Urfa was demolished in a controlled manner), Ajans Urfa Topluluk Kuralları'nı, 15. Sep. 2023. [online] Available at: https://www.ajansurfa.com/haber/16448753/urfada-deprem-de-hasar-goren-su-kulesi-kontrollu-yikildi [Accessed: 11 June 2024] (in Turkish)